CDF/PHYS/BOTTOM/GROUP/8721
Version 0.0
June 5, 2007

# Observation of a Bottom-Strange baryon $\Xi_b$

Dmitry Litvintsev
*Fermi National Accelerator Laboratory*

June 5, 2007

**Abstract**

So far unobserved, bottom baryons containing strange quarks are primarily expected to have long lived charged hyperons, $\Xi^-$ and $\Omega^-$, as one of the decay products. Because of their long lifetime the $\Xi^-$s and $\Omega^-$s are capable of traveling significant distances in the volume of the SVX/ISL detectors and producing hits in silicon strips, before decaying into pairs of $\Lambda^0\pi^-$ and $\Lambda^0 K^-$ respectively. This fact gives a unique opportunity of finding hyperon tracks in the SVX/ISL detectors. The tracking of hyperons in the silicon detector results in a dramatic reduction of the combinatorial background and an improvement of the track position resolution compared with standard reconstruction using just final decay products.

This note describes application of long lived hyperon tracking technique to search for weakly decaying bottom-strange baryons in the $J/\psi\Xi$ decay channel.

Using selection criteria which were obtained in unbiased manner on a control sample of $B^+ \to J/\psi K^+$ decays following verbatim the strategy of $B_c$ search by Fermilab group [4] a significant signal ($> 8.\sigma$) at a mass

$$M = (5,794.0 \pm 3.5(stat) \pm 1.8(syst)) \text{ MeV/c}^2$$

in $J/\psi\Xi$ invariant mass spectrum where $\Xi$ track is reconstructed in SVX. The event yield is $20.1 \pm 4.6$.

This version of the note contains updated results based on sample comprising $\sim 1.9$ fb$^{-1}$ of integrated luminosity (including period 10). There is no change to analysis procedure. A section on mass systematic studies is added.

# Contents

# 1 Introduction

Hadron colliders and $e^+e^-$ machines provided a wealth of fascinating experimental data on bottom mesons. With bottom baryons the experimental situation is not as conclusive. So far only one bottom baryon, the $\Lambda_\mathrm{b}$, has been directly observed in the channels $\Lambda_b \to \Lambda J/\psi$ and $\Lambda_b \to \Lambda_c\pi^-$. Indirect evidence for semileptonic decays of $\Lambda_b$ and $\Xi_b$ exists in the form of enhanced correlations of $\Lambda_c\ell^-$ and $\Xi\ell^-$ observed at LEP and the Tevatron (the latter seen only at the LEP) [11].

Besides the $\Lambda_b$, the quark model predicts multitude of heavy baryon states. This note concentrates on the lowest lying, weakly decaying baryons containing heavy bottom quark and two light quarks, generally referred to as light degrees of freedom (l.d.f.). Some of the properties of these states are summarized in Table 1. The masses of unobserved states are taken from the work of K.G. Körner, D. Pirjol and M. Krämer [7] who used the original non-relativistic potential quark

| Notation | Quark content | $J^P$ | SU(3)(l.d.f.) | $(I, I_3)$ | $S_{ldf}$ | Mass |
|---|---|---|---|---|---|---|
| $\Lambda_b$ | $b[ud]$ | $1/2^+$ | $\bar{\mathbf{3}}_A$ | (0,0) | 0 | $(5624 \pm 9)$ MeV/c$^2$ [11] |
| $\Xi_b^0$ | $b[su]$ | $1/2^+$ | $\bar{\mathbf{3}}_A$ | (1/2,1/2) | 0 | 5.80 GeV/c$^2$ |
| $\Xi_b^-$ | $b[sd]$ | $1/2^+$ | $\bar{\mathbf{3}}_A$ | (1/2,-1/2) | 0 | 5.80 GeV/c$^2$ |
| $\Omega_b^-$ | $bss$ | $1/2^+$ | $\mathbf{6}_S$ | (0,0) | 1 | 6.04 $a$GeV/c$^2$ |

Table 1: Lowest lying $J^P = 1/2^+$ baryon states with B=1 , C=0

model with spin-spin interaction mediated by one gluon-exchange proposed by A. De Rújula, H. Georgi and S. L. Glashow [8] to estimate masses of bottom baryons.

The QCD treatment of quark-quark interactions inside a baryon or meson, significantly simplifies if one of the participating quarks is much heavier compared to the QCD confinement scale $\Lambda_{QCD} \approx 400$ MeV. Therefore it is convenient to calculate properties of heavy hadrons in the limit of infinitely heavy quark mass and then consider power corrections to this limit in terms of systematic $\Lambda_{QCD}/m_Q$ expansion. In the $m_Q \to \infty$ a new kind of symmetry arise – a spin-flavor symmetry or Heavy Quark Symmetry (HQS). HQS provides quantitative description of important aspects of the decays of heavy hadrons that can be subjected to rigorous experimental tests.

The precise measurements of the masses of bottom baryon states will test traditional QCD inspired quark models, quark model with variational approach based on HQS [9] and lattice QCD [10] results. The existing theoretical estimate of lifetime pattern of bottom hadrons is as follows:

$$\tau(\Xi_b^0) \simeq \tau(\Lambda_b) < \tau(B_d) \simeq \tau(B_s) < \tau(\Xi_b^-)$$

with about 7% difference every step of the inequality. The experimental data on $\tau(\Lambda_b)/\tau(B_d) \approx 0.8$ contradicts theoretical prediction, which given all the uncertainty involved, cannot go lower than 0.9. Further experimental studies of bottom baryon lifetimes will help to find out if this contradiction is a temporary difficulty or a more fundamental flaw in our understanding of QCD.

In addition, numerous modes of bottom baryons have the potential to show large CP-violation within the Standard Model. The measurement of CP violation in bottom baryon decays does not require tagging of the initial flavor and time dependence measurement which are necessary in neutral B-system [12].

The extraction of bottom baryon signals is adversely affected by the low production rate as the probability to obtain a baryon in the process of b-quark fragmentation is 10 times lower than the probability to obtain a meson. Bottom baryons decay, often via sequence of decays $b \to$

$c \to s \to u$, producing protons among the final decay products. More abundant bottom mesons decays produce reflections in relevant invariant mass spectra of baryons due to proton/kaon and kaon/pion misidentification complicating background conditions. Therefore, particle identification is a necessary component of baryon studies.

## 2 Decays with charged hyperons in the final state

Fortunately the bottom baryon containing $s$-quarks are primarily expected to have long lived charged hyperons, $\Xi^-$ and $\Omega^-$, as one of the decay products. Below is the list some of the decays and relevant triggers:

- $J/\psi$-trigger:
$$\begin{array}{llll} \Xi_b \to \mathrm{J}/\psi\ \Xi^- + n\pi & , & \Omega_b \to \mathrm{J}/\psi\ \Omega^- + n\pi & \\ \quad\quad\quad\quad \hookrightarrow\ \Lambda\pi^- & & \quad\quad\quad\quad \hookrightarrow\ \Lambda K^- & \end{array}$$
- TTT trigger :
$$\begin{array}{lll} \Xi_b \to\ \ \Xi_c + n\pi & , \Omega_b \to & \Omega_c + n\pi \\ \quad\quad \hookrightarrow\ \Xi^- + n\pi & & \hookrightarrow\ \Omega^- + n\pi \\ \quad\quad\quad \hookrightarrow\ \Lambda\pi^- & & \quad \hookrightarrow\ \Lambda K^- \end{array}$$
$$\Omega_b \to\ \ D^0\Xi^-$$
- SVT track+$\ell$ trigger:
$$\begin{array}{llll} \Xi_b \to\ \ \Xi_c + \ell^-(\pi)X & , \Omega_b \to & \Omega_c + \ell^- X & , \\ \quad\quad \hookrightarrow\ \Xi^- + n\pi & & \hookrightarrow\ \Omega^- + n\pi & \\ \quad\quad\quad \hookrightarrow\ \Lambda\pi^- & & \quad \hookrightarrow\ \Lambda K^- & \end{array}$$

where $n$ denotes 1 or more pions

Because of their long lifetime the $\Xi^-$s and $\Omega^-$s are capable of traveling significant distances in the volume of the SVX/ISL detectors and producing hits in silicon strips, before decaying into pairs of $\Lambda^0\pi^-$ and $\Lambda^0 K^-$ respectively. This fact gives a unique opportunity of finding hyperon tracks in the SVX/ISL detectors. The tracking of hyperons in the silicon detector results in a dramatic reduction of the combinatorial background and an improvement of the track position resolution compared with standard reconstruction using just final decay products. In addition an analysis involving hyperons speeds up dramatically as a complex three-track object is collapsed into a single track that can be combined with other tracks and be subjected to `CTVMFT` vertex fit like any standard track. Unlike a standard track the hyperon track contains a link to information about its decay tracks and the full `CTVMFT` vertex fit information.

The tracking of long lived hyperons has been developed at CDF in 2002-2003 and is extensively documented in CDF note 6527 [1]. In the past the benefits of hyperon tracks were utilized when searching for exotic S=-2 states decaying to $\Xi\pi$ [2].

This note describes application of long lived hyperon tracking technique to search for weakly decaying bottom-strange baryons in the following decay channel:

- $\Xi_b^- \to J/\psi\Xi$
- $\Xi_b^- \to \Xi_c^0\pi^-$
- $\Xi_b^0 \to \Xi_c^+\pi^-$

The search is based on the data sample comprising integrated luminosity of $\sim 1.9$ fb$^{-1}$ collected by CDF during time period of up to 30 Jan 2007.

## 3 Datasets

The handling of datasets containing data from $J/\psi$, TTT and SVT+$\ell$ triggers follows a similar path to one described in our previous notes [1, 2].

An executable `JpsiXFind` which is built in `JpsiXMods` package contains two essential modules – `SecVtxModule` and `Hyperon` (both are part of `JpsiXMods` package). The `SecVtxModule` module finds $\Lambda^0$s (or $K_S^0$ depending on `talk-to` switch) candidates passing very loose selection criteria and appends them to the `EventRecord` in the form of track view. This track view is picked by `Hyperon` module downstream. The `Hyperon` module is the hyperon tracking module. It performs the following actions.

- Extracts $\Lambda$ decay tracks from `CdfTrackView` object created in the previous step by the `SecVtxModule`.
- Loops over $\Lambda^0$ candidates decay tracks attaching additional third track assumed to be pion (or kaon depending on `talk-to` choice of hyperon). Sets up `CTVMFT` 1-track pointing constraint fit of $\Xi$ candidate vertex.
- Performs vertex constraint `CTVMFT` fit of $\Xi$ candidates. The momentum and decay vertex position of the $\Xi$ candidate determined after fit are used to define its track helix. The $\Xi$ track parameters $(\lambda, cu, z_0, d_0, \phi_0)$ and $5 \times 5$ track covariance matrix is properly re-calculated from $\Xi$ momentum, vertex position and elements of `CTVMFT` error matrix `VMAT`. Hits in the SVX/ISL detector made by real $\Xi$ hyperons are expected to fall near the extrapolation of this "COT" track in the silicon detectors. A modified OI(Z) tracking algorithm is used to attach hits in the SVX/ISL to the $\Xi$ helix, which required a minimum of two axial silicon hits. The hyperon tracks found in the SVX/ISL are used, with $\Xi$ mass assignment, in the subsequent analyzes the same as the standard tracks produced by stable particles.
- Appends the COT and Silicon hyperon track collections and hyperon `CTVMFT` fit results associated with each track are to the `EventRecord`.

The analysis proceeds in two stages. The first stage is time consuming and involves routine running of the `JpsiXFind` executable on the input data containing triggers of interests and a collection of datasets is created, each of which contain hyperon track collections. Table 2 contains information about available datasets. As of today, only $J/\psi$-trigger, TTT trigger and SVT+$\mu$

| Name | id | parent dataset id | trigger |
|---|---|---|---|
| XI_JPSI-0d | x6nx1d | xpmm0d | $J/\psi$-trigger |
| XI_JPSI-0e | x6nx0e | xpmm0e | $J/\psi$-trigger |
| XI_JPSI-2h | x6nx2h | xpmm0h,xpmm0i | $J/\psi$-trigger |
| XI_TRACKED_MASS_FIT-0d | x6nx2d | xbhd0d | TTT trigger |
| XI_TRACKED_MASS_FIT-0e | x6nx1e | xbhd0e | TTT trigger |
| XI_TRACKED_MASS_FIT-0h | x6nx3h | xbhd0h,xbhd0i | TTT trigger |
| XI_TRACKED_NO_MASS_CONSTRAINT_SVT_MU-0d | x6nx5d | xmbu0d, xbmu0h,xbmu0i | SVT+$\mu$ trigger |
| XI_TRACKED_NO_MASS_CONSTRAINT_SVT_E-0d | x6nx6d | xbel0d, xbel0h,xbel0i | SVT+$e$ trigger |

Table 2: Datasets containing hyperon tracks

trigger are complete and contain data corresponding to integrated luminosity of about 1.9 $\text{fb}^{-1}$.

At the second stage of the analysis a fast job is run over the produced datasets. Different modules of the same `JpsiXFind` executable extract hyperon tracks from the event and combine them with other tracks to form $\Xi_b$ candidates. The results are ntupelized and analyzed in normal fashion.

# 4 Selection of hyperons

## 4.1 The $\Lambda$ hyperon selection

$\Lambda$ hyperons were reconstructed from opposite charge pairs of tracks satisfying "default track" criteria. The track with higher $\mathrm{p_T}$was assigned the proton mass and track with lower $\mathrm{p_T}$was assigned the pion mass. The track pairs having $|\Delta \mathrm{z}| < 5$ cm and $\mathrm{M(p\pi^-)} < 1.16$ GeV/c$^2$ at the intersection point were subjected to a vertex fit with $\chi^2_{r-\phi} < 49$. In addition, we required $\Lambda$ flight distance in the transverse plane to be greater than 1 cm, and $\cos(\alpha) > 0.5$, where

$$\cos(\alpha) = \frac{\vec{p_\Lambda} \cdot \vec{d_\Lambda}}{|\vec{p_\Lambda}| \cdot \left|\vec{d_\Lambda}\right|},$$

and $\vec{d_\Lambda}$ is the vector which points from the primary to the $\Lambda$ decay vertex. These cuts are extremely soft.

## 4.2 $\Xi$ reconstruction and tracking

$\Xi$ hyperons were reconstructed in the decays to $\Lambda\pi^-$ pairs. The combination of the neutral particle and the charged track in the final state suggests a convenient method of using wrong charge combinations ($\Lambda\pi^+$) to model *uncorrelated* background to $\Lambda\pi^-$. Having selected a $\Lambda$ hyperon, the probability to combining it with a random track is the same for negative and positive tracks, neglecting small effects due to the difference in COT efficiency for positive and negative tracks. Therefore, for inclusive hyperon studies, both right and wrong charge combinations were selected.

The $(p\pi^-)$ pairs satisfying the $\Lambda$ selection criteria and having an invariant mass, calculated at the tracks intersection point, to be within a $\pm 5$ MeV/c$^2$ window around nominal $\Lambda$ mass, were combined with all remaining pions in the event. The resulting three track candidates were subjected to the following procedure:

- Vertex fit with the $(p\pi^-)$ mass constrained to PDG value of 1.1156 GeV/c$^2$. The $\Lambda$ vertex was constrained to point back to $\Xi$ candidate vertex with the 1-track constraint. No fit quality cuts were imposed.
- If the fit was successful, then the $(p, \pi^-)+\pi^\pm$ combinations with invariant mass within 60 MeV/c$^2$ window around $\Xi$ PDG mass were mass constrained[1] to that value and refit. No fit quality cuts were imposed.
- The distance to $\Lambda$ decay vertex to exceed the $\Xi$ flight distance by 1 cm in the transverse plane.

Additional cuts imposed on $\Xi$ candidates were obtained in the process of maximizing the significance with respect to the cut described in CDF 6527 [1]. Namely:

[1]In the SVT+$\ell$ datasets the mass constraint on $\Xi$ was not used

- for $\Lambda$ decay daughters $|d_0(p)| > 0.05$ cm and $|d_0(\pi)| > 0.05$ cm where $d_0$ is track impact parameter with respect to the beam pipe
- $|d_0(\Xi)| < 0.1$ cm

Only $\Xi$ tracks found in silicon are used in the subsequent analysis. The cuts chosen for $\Xi$ tracks are frozen and won't change to search for bottom-strange baryons.

# 5 Observation of $\Xi_b \to J/\psi\Xi$

The $\Xi_b^- \to J/\psi\Xi$ decay mode seems like the most straightforward discovery mode [2]. A cartoon depicting decay topology is shown in Figure 1. There are two trigger muons from $J/\psi$ decay plus SVX hyperon track, i.e. three track final state which is similar to the decay $B^+ \to J/\psi K^+$. Therefore the high statistics $B^+ \to J/\psi K^+$ sample is used as a reference mode to optimize cuts specific to 3-track final state, like 3D vertex fit probability and vertex separation as the lifetimes of $\Xi_b^-$ and $B^+$ are expected to be similar. The expected yield in of $\Xi_b^-$ is estimated from known

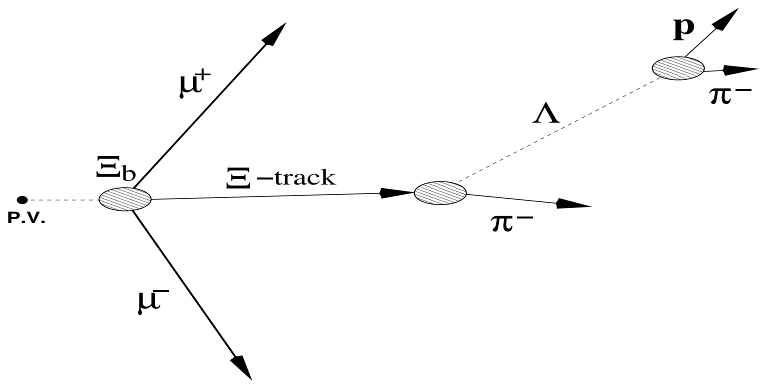


Figure 1: Decay signature of $\Xi_b \to J/\psi\Xi$ decays triggered by $J/\psi$-trigger

yield of $\Lambda_b \to J/\psi\Lambda$ and measured b-quark fragmentation fractions into mesons and baryons [11]:

$$bu \ : \ bd \ : \ bs \ : \ b - baryon = 0.388 : 0.388 : 0.106 : 0.118.$$

Assuming that the probability of s-quark popping is the same for baryons and mesons one gets:

$$bud \ : \ bsd \ : \ bsu \ : \ bss = 0.78 : 0.098 : 0.098 : 0.024.$$

Assuming $\mathcal{B}(\Lambda_b \to J/\psi\Lambda) = \mathcal{B}(\Xi_b^- \to J/\psi\Xi)$ :

$$N(\Xi_b^- \to J/\psi\Xi) \sim \frac{N(\Lambda_b \to J/\psi\Lambda)}{8.3} \cdot \frac{A(\Xi_b^-)}{A(\Lambda_b)} \cdot \epsilon_{SVX} \sim \frac{N(\Lambda_b \to J/\psi\Lambda)}{8.3} \cdot 0.9 \cdot \epsilon_{kink-\pi} \cdot \epsilon_{SVX},$$

where

| | | |
|---|---|---|
| $\frac{A(\Xi_b^-)}{A(\Lambda_b^-)}$ | =0.9 | is detector and trigger acceptance ratio obtained using PYTHIA |
| $\epsilon_{kink-\pi}$ | =0.8 | optimistic estimate of pion efficiency from $\Xi \to \Lambda\pi$ decay |
| $\epsilon_{SVX}$ | =0.4 | known relative hyperon SVX track efficiency. |

[2] The neutral isospin partner $\Xi_b^0$ decaying to $\Xi_b \to J/\psi\Xi^0$, followed by $\Xi^0 \to \Lambda\pi^0$ is hopelessly lost at CDF

Therefore:

$$N(\Xi_b^- \to J/\psi\Xi) \sim \frac{N(\Lambda_b \to J/\psi\Lambda)}{30}.$$

So, provided low amount background, the signal of 15-20 events should be statistically significant in 1.9 $fb^{-1}$ sample.

### 5.1 Analysis strategy

As it has been noted above, a decay $B^+ \to J/\psi K^+$ is used as a control sample. The idea is to obtain the cuts that allow to extract clean $B^+$ signal while retaining high signal selection efficiency. Having fixed the cuts, apply the cuts blindly to $J/\psi\Xi$ candidates and open the box.

The expected mass resolution of the $\Xi_b$ is determined using full GEANT Monte Carlo simulation of the PYTHIA input events $p\bar{p} \to \Xi_b X$ where $\Xi_b$ were allowed to decay to $J/\psi\Xi$. The same reconstruction and analysis procedure is applied to the simulated events as was applied to the data.

The invariant mass spectrum of $J/\psi\Xi$ is kept blind until the cuts are determined in $B^+ \to J/\psi K^+$ control signal. The signal region is defined generously to include a wide range of mass predictions:

- $\Xi_b$ signal region: $|M(J/\psi\Xi) - 5.82| < 0.1$ GeV/c$^2$
- $\Xi_b$ left sideband : $|M(J/\psi\Xi) - 5.62| < 0.1$ GeV/c$^2$
- $\Xi_b$ right sideband : $|M(J/\psi\Xi) - 6.02| < 0.1$ GeV/c$^2$.

The expected background level in the signal region is determined using extrapolation from sideband regions. Once the signal box is opened, the number of observed events in the box is compared to the number of expected events and a probability of background fluctuation to this number is determined (p-value). If the signal is significant, that is corresponds to more than 5 Gaussian sigmas, proceed to fit the signal with Gaussian shape of fixed width equal to expected detector mass resolution to determine central value of the mass. The systematic uncertainty of the mass scale is determined by looking to well established signals containing $\Xi$ tracks and comparing central values of the masses with world averaged masses and scaling the observed differences by the decay $Q$-value ratio.

#### 5.1.1 Unbiased selection criteria choice

An example analysis exists that emphasized the removal of the background by tuning selection requirements in the data on the $B^+ \to J/\psi K^+$ signal. This is the search for exclusive $B_c^+ \to J/\psi\pi^+$ by Lukens, Tkaczyk and Wester described in CDF note 7572 [4]. The cuts chosen, are obtained in an unbiased way on the data using $B^+ \to J/\psi K^+$ signal and a new particle is found by applying these cuts to the $B_c^+ \to J/\psi\pi^+$ decay. Even given expected shorter lifetime of $B_c$ the method turned out to be a success. For the $\Xi_b$ it should work even better given similar expected lifetimes of $B^+$ and $\Xi_b$.

The CDF note 7572 [4] describes a successful application of a decision tree algorithm with specific cut values motivated by CDF experience in reconstruction of $B^+ \to J/\psi K^+$. That is, two set of cuts are tried – a loose set of cuts, called Optimization A, and a tighter set of cuts, called Optimization B. A $B^+$ candidate is accepted if it passes Optimization A cuts. If it fails just one Optimization A cut, then tighter cuts of Optimization B are applied and if the candidate passes all of the them minus the cut on variable it failed in Optimization A, the candidate is accepted. This strategy allows to recover up to 30% of candidates that fail just one Optimization A cut.

Table 3 lists the loose (Optimization A) and tight (Optimization B) cuts taken verbatim from the CDF note 7572 [4]. The goal of this analysis is to re-produce $B^+$ yields with these cuts to make sure there are no problems with analysis modules and then apply these same cuts blindly to $J/\psi\Xi$ candidates. Due to purely technical reasons there will be one exception to the cuts listed in Table 3.

| Selection variable | Optimization A | Optimization B |
|---|---|---|
| $p_T(K)$ [GeV/c] | $> 1.7$ | $> 2.5$ |
| $p_T(J/\psi K)$ [GeV/c] | $> 5.$ | $> 6.$ |
| $ct(J/\psi K)$ [cm] | $> 0.008$ | $> 0.01$ |
| $\delta[ct(J/\psi K)]$ [cm] | $< 0.003$ | $< 0.0025$ |
| Pointing angle | $< 0.4$ radians | $< 0.3$ radians |
| $prob(\chi^2(3D))$ | $> 10^{-3}$ | $> 10^{-2}$ |
| $\|d_0(K)\|$ (w.r.t sec vtx.) [cm] | $< 0.01$ | $< 0.008$ |
| $\|d_0(K)_{sig}\|$ (w.r.t. p.v.) | $> 2.5\sigma$ | $> 3.0\sigma$ |
| $\|d_0(J/\psi K)_{sig}\|$ (w.r.t. p.v.) | $< 2.5\sigma$ | $< 2.0\sigma$ |

Table 3: Selection variables and requirements for Optimization A and Optimization B taken verbatim from CDF 7572

### 5.2 Offline tracks and Alignment table

- ProcessName is set to `PROD_PHYSICS_CDF` and PassName 17 as input parameters to the `CalibrationManager`.
- AlignmentSource set to "default" in `GeometryManager`.
- Additional layers of material were added to the silicon geometry according to the note [5].
- Default tracks were required to have at least 10 COT stereo hits and 10 COT axial hits, and more then 2 axial silicon hits (for $\mu, K$ tracks )
- To correct for the energy losses and multiple scattering in the silicon detector tracks were refit using Kalman refitter taking into account appropriate masses for different candidates ($K$,$\pi$, $p$ and $\mu$) participating in decay chains under study
- The COT covariance matrix was rescaled with scaling factors 21.72, 11.57, 14.64, 1.71, 1.544 for curvature, $d_0$, $\phi_0$, $z_0$, and $\lambda$, accordingly.
- The COT track curvature was rescaled using the `corrCOT()` method of `TrackRefitter` to correct for energy losses in the COT volume.

### 5.3 Good run list

No good run list requirements were applied.

### 5.4 Muon selection

Muons of all types are accepted for the analysis. An event has to have at least 2 muon candidates filtered from default from `CdfMuonView` returned by `CdfMuonView::defMuons()` by applying the following cuts:

- all types of muons are accepted
- for CMU muons, the $\chi^2_x$ of track-stub match was required to be $\chi^2_x \leq 9$
- for CMX muon, the $\chi^2_x$ of track-stub match was required to be $\chi^2_x \leq 9$
- number of axial SVX hits was required to exceed 2 $N(r-\phi) > 2$
- the energy measured in the electromagnetic calorimeter associated with muon was required to be $E_{EM} < 4$ GeV
- the energy measured in the hadronic calorimeter associated with muon was required to be $E_{HAD} < 8$ GeV.
- $p_T(\mu) > 1.5$ GeV/c.

### 5.5 $B^+ \to J/\psi K^+$ signal in 1.9 fb$^{-1}$

The input datasets used for this sub-analysis were : xpmm0d, xpmm0h, xpmm0i. Run range up to 233111. The amount of data corresponds to approximately 1.9 fb$^{-1}$. Figure 2 shows an invariant mass spectrum of di-muon candidates surviving `CTVMFT` vertex fit with fit probability, $prob(\chi^2(3D)) > 10^{-3}$. Having defined $J/\psi$ sidebands as follows:

- $J/\psi$ signal region : $|m(\mu\mu) - m(J/\psi)| < 3 \cdot 0.018$ GeV/c$^2$
- $J/\psi$ sideband region: $5 \cdot 0.018 < |m(\mu\mu) - m(J/\psi)| < 8 \cdot 0.018$ GeV/c$^2$,

the $J/\psi$ yield in 1.9 fb$^{-1}$ of data was determined using sideband subtraction. The yield turned out to be $15,157,315 \pm 4149$.

Figure 3 shows invariant mass spectrum of $J/\psi K^+$ candidates passing minimal pre-selection cuts:

- $|m(\mu\mu) - m(J/\psi)| < 0.048$ GeV/c$^2$ (this cut differs of usual window size of $\pm 80$ MeV/c$^2$ applied at CDF, as a result of oversight rather than intentional)
- `CTVMFT` mass constrained (on $J/\psi$ candidate) vertex fit with $prob(\chi^2(3D)) > 10^{-4}$
- $p_T(J/\psi K^+) > 5.0$ GeV/c.
- $p_T(K^+) > 1.0$ GeV/c.

A smooth curve superimposed on the plot shows fit to the sum of single Gaussian signal term and polynomial background. The fit yielded $31,652 \pm 567$ events in the peak at a mass of $(5,278.0 \pm 0.2)$ MeV/c$^2$. The mass resolution $\sigma = (11.2 \pm 0.2)$ MeV/c$^2$. The arrows mark $B^+$ signal and sideband regions were defined as:

- $B^+$ signal region: $|m(J/\psi K^+) - m(B^+)| < 3\sigma$ GeV/c$^2$

- $B^+$ sideband region: $7\sigma < |m(J/\psi K^+) - m(B^+)| < 10\sigma$ GeV/c$^2$.

The position of the sideband was chosen to fit between the main $B^+$ peak and irreducible feed downs from partially reconstructed $B \to J/\psi KX$ decays which are present at the masses $M(J/\psi K^+) < 5.15$ GeV/c$^2$ and fully Cabibbo suppressed decay $B^+ \to J/\psi \pi^+$ which creates prominent shoulder at just to the right of $B \to J/\psi K^+$ signal. The width of sideband region is chosen to match the width of signal region.

At this point the cuts from Table 3 were about to be applied to $B^+ \to J/\psi \pi^+$ candidates. Although, looking at the content of the analysis ntuples, a deficiency has been discovered. It turned out that a correct significance of a $B^+$ candidate's impact parameter with respect to the primary vertex could not be properly calculated as error matrix of primary vertex position was missing in the ntuple. To account for that, a cut on "$|d_0(J/\psi K)_{sig}|$ (w.r.t p. v.)" used in $B_c$ search is replaced by equivalent cut on absolute value of $B^+$'s signed impact parameter. To chose the value of this cut, the sideband subtracted distribution of $d_0(J/\psi K)$, obtained with minimal set of pre-selection cuts, has been studied. It is shown in Figure 4. A smooth function shows result of the fit to single Gaussian resolution function. The fit yielded $\sigma(d_0(J/\psi K^+) = (32 \pm 0.1)\ \mu$m. Therefore the the cuts on $B^+$ impact parameter significance were replaced as follows:

- Optimization A: $|d_0(J/\psi K)_{sig}| < 2.5\sigma \to |d_0(J/\psi K)| < 75\ \mu$m
- Optimization B: $|d_0(J/\psi K)_{sig}| < 2.0\sigma \to |d_0(J/\psi K)| < 60\ \mu$m

Table 4 summarized the cuts that will be applied to $B^+ \to J/\psi K^+$ candidates. Figures 5 shows a

| Selection variable | Optimization A | Optimization B |
|---|---|---|
| $p_T(K)$ [GeV/c] | $> 1.7$ | $> 2.5$ |
| $p_T(J/\psi K)$ [GeV/c] | $> 5.$ | $> 6.$ |
| $ct(J/\psi K)$ [cm] | $> 0.008$ | $> 0.01$ |
| $\delta[ct(J/\psi K)]$ [cm] | $< 0.003$ | $< 0.0025$ |
| Pointing angle | $< 0.4$ radians | $< 0.3$ radians |
| $prob(\chi^2(3D))$ | $> 10^{-3}$ | $> 10^{-2}$ |
| $\|d_0(K)\|$ (w.r.t sec vtx.) [cm] | $< 0.01$ | $< 0.008$ |
| $\|d_0(K)_{sig}\|$ (w.r.t. p.v.) | $> 2.5\sigma$ | $> 3.0\sigma$ |
| $\|d_0(J/\psi K)\|$ [cm] | $< 0.0075$ | $< 0.006$ |

Table 4: Selection variables and requirements for Optimization A and Optimization B used in this analysis.

column of three plots showing mass spectra of $J/\psi K^+$ candidates passing optimized selection criteria. From top to bottom: Optimization A, Optimization B and the sum of the two. All spectra demonstrate excellent signal to background ratios. All three spectra we fit with a function consisting of single Gaussian signal term and linear polynomial background. Fits are of poor quality as they do not describe Cabibbo suppressed $B^+ \to J/\psi$ contribution prominently visible as higher mass shoulders to the main $B^+$ peaks. The precise numbers of events are of secondary concern as the ballpark numbers are of interest to have an estimate of signal selection efficiency. Table 5 summarizes the yields. Optimization A+B retains about 50% of $B^+$ signal while background is cut by the factorof 500! The $B^+$ yields are consistent with findings in CDF 7572 taking into account difference in luminosity (a factor of 1.5).

| Minimal Cuts | Optimization A | Optimization B | Optimization A+B |
|---|---|---|---|
| $31,652 \pm 567$ | $11,639 \pm 110$ | $3,807 \pm 63$ | $15,432 \pm 127$ |

Table 5: $B^+$ yields obtained in different cut

Following a specific request during pre-blessing an attempt has been made to accurately describe $J/\psi K^+$ invariant mass spectra obtained after applying optimization cuts. Following a recipe developed to measure a ratio of branching ratios $\mathcal{B}(B^+ \to J/\psi\pi^+)/\mathcal{B}(B^+ \to J/\psi K^+)$ [6] a 2D event-by-event fit has been performed. The fit PDF consisted of two signal terms describing Cabibbo-allowed decay $B^+ \to J/\psi K^+$ and Cabibbo suppressed decay $B^+ \to J/\psi\pi^+$ and second order polynomial background. The fit range was chosen to be [5.2,5.5] to avoid low mass shoulder created by inclusive $B \to J/\psi X$ decays.

A contribution from the Cabibbo-suppressed decay $B^+ \to J/\psi\pi^+$ is modelled by Gaussian centered at

$$M_1 = \sqrt{M^2(B^+) + (1+\alpha)(m_K^2 - m_\pi^2)},$$

where $\alpha = \dfrac{E(J/\psi)}{p_K}$. The main decay $B^+ \to J/\psi K^+$ signal is described by the sum of two Gaussians centered at $M(B^+)$. The width of a narrow Gaussian describing $B^+ \to J/\psi K^+$ and the width of the Gaussian describing $B^+ \to J/\psi\pi^+$ were set to be equal. The fit was performed with all parameters floating. The relevant fit results are listed in Table 6 : The $B^+$ signal parameters

| parameter | Optimization A | Optimization B | Optimization A+B |
|---|---|---|---|
| $N(J/\psi K^+)$ | $12,185 \pm 115$ | $3,837 \pm 67$ | $16,044 \pm 134$ |
| $N(J/\psi\pi^+)$ | $447 \pm 29$ | $134 \pm 18$ | $572 \pm 34$ |
| $M(B^+)$ [MeV/c$^2$] | $5,278.3 \pm 0.1$ | $5,278.3 \pm 0.2$ | $5,278.3 \pm 0.1$ |
| $\sigma_1$ [MeV/c$^2$] | $28.6 \pm 1.4$ | $26.5 \pm 2.2$ | $27.8 \pm 1.2$ |
| $\sigma_2$ [MeV/c$^2$] | $11.0 \pm 0.1$ | $10.3 \pm 0.1$ | $10.8 \pm 0.1$ |
| $R$ (fraction of wide Gaussian) | $0.17 \pm 0.02$ | $0.24 \pm 0.05$ | $0.19 \pm 0.02$ |

Table 6: $B^+$ parameters obtained using unbinned event-by-event fit described in [6].

(widths and the fractions of narrow and wide Gaussians) are in good agreement with the MC predictions listed in table 8 (see Section 5.8 below).

### 5.6 $\Lambda_b^0 \to J/\psi\Lambda^0$ signal in 1.9 fb$^{-1}$

Since $B^+ \to J/\psi K^+$ decay does not contain $\Lambda^0$ as oone of the decay products we performed cross-check of our $\Lambda$ selection by looking for $\Lambda_b \to J/\psi\Lambda^0$ candidates. The input datasets used for this sub-analysis were the same as for $B^+$ study: xpmm0d, xpmm0h, xpmm0i. Run range up to 228596. The amount of data corresponds to approximately 1.9 fb$^{-1}$. Figure 7 shows an invariant mass spectrum $J/\psi\Lambda^0$ passing the cuts very similar to ones used in $\Lambda_b$ lifetime paper [13]. The $\Lambda^0$ candidates were formed as previously described. No mass constraint fit was applied to $\Lambda$ candidates. Additional cuts are listed in Table 7. Am un-binned event by event fit to a single Gaussian plus liner background resulted in $470 \pm 25$ candidates at the mass of $(5,619.2 \pm 0.7)$ MeV/c$^2$. The mass is in excellent agreement with previous CDF II work [14].

| Selection Criterion |
|---|
| $1.105 < M(p\pi) < 1.125$ MeV/c$^2$ |
| $3.014 < M(\mu\mu) < 3.174$ MeV/c$^2$ |
| $p_T(\Lambda) > 2.6$ GeV/c |
| $\frac{L_{xy}(\Lambda)}{\sigma_{L_{xy}(\Lambda)}} > 4$ |
| $chi^2(3D) < 25$ |
| $ct(J/\psi\Lambda) > 0.02$ cm |
| $p_T(J/\psi\Lambda) > 4.5$ GeV/c |

Table 7: Selection criteria used to select $\Lambda_b \to J/\psi\Lambda$ candidates.

### 5.7 $\Xi$ signals in $J/\psi$ trigger

Having established selection procedure independently from the decay under study it is time to turn to $\Xi$ signal in $J/\psi$ trigger data. The datasets used for this study were x6nx1d, x6nx0e, x6nx2h (see Table 2). The invariant mass spectrum of $\Lambda\pi$ combinations having associated silicon $\Xi$ track is shown in Figure 9.

A bump at M=1.275 GeV/c$^2$ is explained in detail in our previous note [1]. It is caused by self-reflection on real $\Xi$ candidate which have both pions satisfying $\Lambda$ mass window. That is if we label pions like this $\Xi \to \Lambda^0\pi_1$, followed by $\Lambda^0 \to p\pi_2$, then if both $|m(p\pi_1) - M(\Lambda)| < 10$ MeV/c$^2$ and $|m(p\pi_2) - M(\Lambda)| < 5$ MeV/c$^2$, then an artificial structure is generated by at the mass centered at 1.275 GeV/c$^2$in the $\Lambda\pi^-$ invariant mass spectrum which is not reproduced in wrong charge spectrum of $\Lambda\pi^+$ due to obvious absence of real $\Xi$ candidates in the wrong charge sample. Still the wrong charge combination is a useful tool showing that no artificial $\Xi$ signal is generated by the vertex fitting with mass constrains or SVX hyperon tracking.

The sample of $\Xi$ silicon tracks available for this analysis is $23,500 \pm 342$ candidates. The yield has been determined by fitting wrong change subtracted $\Lambda\pi$ mass spectrum to the function consisting of two Gaussian signal terms and a polynomial. The procedure is similar to one described in [1]. It is important that the fitted mass of the $\Xi$ is consistent with PDG indicating that no artificial bias has been created by the hyperon tracking and selection procedures.

### 5.8 Monte Carlo studies

The major assumption of this analysis is that decays $\Xi_b \to J/\psi\Xi^-$ and $B^+ \to J/\psi K^+$ are similar allowing one to obtain optimal cuts for $\Xi_b \to J/\psi\Xi^-$ search on the independent, high statistics calibration sample of $B^+ \to J/\psi K^+$ candidates. A way to check the validity of this assumtion is to use Monte Carlo samples for both decays. If simulated events look simlilar one can extrapolate that the similarity holds true for the real data as well.

Several samples were generated using BGENERATOR package. Subsequent simulation included full GEANT and trigger simulation chain followed by Production executable. CDF software version 6.1.4mc has been used. Three species of bottom hadrons were generated – $B^+$, $\Lambda_b^0$ and $\Xi_b^-$ 1,000,000 events each. They were decayed using `EVTGEN` decay package to $J/\psi K^+$, $J/\psi\Lambda^0$ and $J/\psi\Xi^-$ respectively. Long lived hyperons – $\Lambda^0$ and $\Xi^-$ were decayed inside detector by GEANT. The $\Lambda^0$ branching ratio to $p\pi^-$ was left unchanged. We used default lifetimes and production spectra (default lifetimes for all B-species are equal to $1.5 \cdot 10^{-12}s$).

The candidates were selected by applying Optimization A+B cuts to $B^+$ and $\Xi_b^-$. The $\Lambda_b^0$ candidates were selected by applying cuts taken from $\Lambda_b$ lifetime paper [13] (see above).

Figures 10 and 11 show plots of 9 variables being cut on in Optimizatopn A and B. Each plot contains two histograms, normalized to the same are. Histograms with error bars correspond to $B^+$; the solid line histograms show $\Xi_b^-$. Apart from obvious difference between $p_T(K)$ and $p_T(\Xi)$ spectra due to heavier mass of the latter, the distributions are remarkably similar, or, generally speaking similar enough to trust that Optimization A+B procedure would work for $\Xi_b^-$ signal in the data.

Another sequence of mandatory plots shown in Figures 12-18 shows excellent agreement between simulation and the $B^+$ data. In all these plots the real data are represented by histograms with error bars and simulated data are shown with solid line histograms.

| Channel | yield | mass resolution(s) [MeV/c$^2$] | input mass [MeV/c$^2$] | measured mass [MeV/c$^2$] | $\Delta$ [MeV/c$^2$] |
|---|---|---|---|---|---|
| $B^+ \to J/\psi K^+$ | $27,108 \pm 166$ | $\sigma_1 = 33.6 \pm 1.4$<br>$\sigma_2 = 10.95 \pm 0.09$<br>$R = 0.109 \pm 0.008$ | $5,277.6$ | $5,278.75 \pm 0.08$ | $1.15 \pm 0.08$ |
| $\Lambda_b^0 \to J/\psi \Lambda^0$ | $5,033 \pm 71$ | $\sigma_1 = 27.4 \pm 2.2$<br>$\sigma_2 = 11.64 \pm 0.26$<br>$R = 0.15 \pm 0.03$ | $5,640.0$ | $5,640.9 \pm 0.2$ | $0.9 \pm 0.2$ |
| $\Xi_b^- \to J/\psi \Xi^-$ | $1,791 \pm 42$ | $\sigma_1 = 34.0 \pm 1.7$<br>$\sigma_2 = 12.23 \pm 0.66$<br>$R = 0.62 \pm 0.11$ | $5,580.0$ | $5,802.3 \pm 0.4$ | $2.3 \pm 0.4$ |

Table 8: Masses and resolutions obtained from BGENERATOR MC samples. $B^+$ and $\Xi_b^-$ candidates were selected in Optimization A+B cuts. The $\Lambda_b^0$ candidates were selected using cuts from $\Lambda_b^0$ lifetime paper [13]. Parameter $R$ is the fraction of "wide" Gaussian.

Analysis of invariant mass spectra of $J/\psi K^+$, $J/\psi\Xi$ and $J/\psi\Lambda$ reveals a complex signal structure. We were able to describe signals with double Gaussians. Figures 20-22 show projections of unbinnes double Gaussian fits to invariant mass spectra of $J/\psi K^+$, $J/\psi\Lambda$ and $J/\psi\Xi$. Gaussians widths are similar, but the fraction of wide Gaussian varies form the lowest for $J/\psi K^+$ to the highest for $J/\psi\Xi$. The fit results are summarized in Table 8. Mass difference between observed and generated mass is also quoted. The mass differences are $(1.15 \pm 0.08)$ MeV/c$^2$ for $B^+$, $(0.9 \pm 0.2)$ MeV/c$^2$ for $\Lambda_b^0$ and $(2.3 \pm 0.4)$ MeV/c$^2$ for $\Xi_b$.

Table 9 summarizes individual cut efficienies of Optimization A and Optimization B selections obtained on simulated $B^+$ and $\Xi_b^-$ samples.

### 5.9 $\Xi_b \to J/\psi\Xi$

All silicon $\Xi$ tracks were combined with $J/\psi$ di-muon candidates to form 3-track displaced vertex and were subjected to `CTVMFT` vertex with with mass constraint on $J/\psi$. The $J/\psi$ mass window was : $|m(\mu\mu) - M(J/\psi)| < 0.080$ GeV/c$^2$ – a standard cut in CDF. Before applying Optimization A+B cut, we looked at the invariant mass plot of $J/\psi\Xi$ candidates with blinded signal region $|m(J/\psi\Xi) - 5.82| < 0.1$ GeV/c$^2$, obtained with minimum selection requirements. In this case, in addition to all cuts listed in Table 10, the minimum requirement is the only cut on $prob(\chi^2(3D)) > 10^{-4}$ of `CTVMFT` fit.

Figure 23 shows $M(J/\psi\Xi)$ spectrum with blinded signal region. The search for $\Xi_b$ is not blind, and we intend to open the box once the cuts listed in Table 11 are applied.

| | $B^+$ | | $\Xi_b^-$ | |
|---|---|---|---|---|
| Selection variable | Optimization A | Optimization B | Optimization A | Optimization B |
| $p_T(K/\Xi)$ | $0.6324 \pm 0.0018$ | $0.4530 \pm 0.0019$ | $0.9866 \pm 0.0019$ | $0.9040 \pm 0.0049$ |
| $p_T(J/\psi K/\Xi)$ | N.A. | $0.8375 \pm 0.0014$ | N.A. | $0.9294 \pm 0.0042$ |
| $ct(J/\psi K/\Xi)$ | $0.8532 \pm 0.0013$ | $0.8198 \pm 0.0014$ | $0.8243 \pm 0.0063$ | $0.7818 \pm 0.0068$ |
| $\delta[ct(J/\psi K/\Xi)]$ | $0.5416 \pm 0.0019$ | $0.3674 \pm 0.0018$ | $0.7259 \pm 0.0074$ | $0.5521 \pm 0.0082$ |
| Pointing angle | $0.9190 \pm 0.0010$ | $0.8960 \pm 0.0011$ | $0.9013 \pm 0.0049$ | $0.8713 \pm 0.0055$ |
| $prob(\chi^2(3D))$ | $0.9400 \pm 0.0009$ | $0.8656 \pm 0.0012$ | $0.6839 \pm 0.0077$ | $0.5802 \pm 0.0082$ |
| $\|d_0(K/\Xi)\|$ (w.r.t sec vtx.) | $0.9363 \pm 0.0009$ | $0.9079 \pm 0.0011$ | $0.9836 \pm 0.0021$ | $0.9779 \pm 0.0024$ |
| $\|d_0(K/\Xi)_{sig}\|$ (w.r.t. p.v.) | $0.7003 \pm 0.0017$ | $0.6582 \pm 0.0018$ | $0.7520 \pm 0.0071$ | $0.7076 \pm 0.0075$ |
| $\|d_0(J/\psi K/\Xi)\|$ (w.r.t. p.v.) | $0.9683 \pm 0.0007$ | $0.9235 \pm 0.0010$ | $0.9531 \pm 0.0035$ | $0.9059 \pm 0.0048$ |

Table 9: Individual cut efficiencies of Optimization A and Optimization B selections obtained on simulated $B^+$ and $\Xi_b^-$ samples

.

Figure 24 shows $M(J/\psi\Xi)$ spectra. From top to bottom: Optimization A, Optimization B and Optimization A+B.

### 5.10 Mass measurement

The $M(J/\psi\Xi)$ candidates were subjected to unbinned log likelihood mass fit. The following function was minimized:

$$F = -2\ln\mathcal{L} = n + a_0(x_{max} - x_{min}) - \sum_{i=1}^{N} f(x_i, M_0, \sigma_M, a_0)$$

where $x_{min} = 5.25$ GeV/c$^2$ and $x_{max} = 6.5$ GeV/c$^2$ and $f(x_i, M_0, \sigma_M, a_0)$ is a sum of Gaussian signal term and constant background:

$$f(x_i, M_0, \sigma_M, a_0) = \mathcal{G}(x_i, \sigma, M_0) + a_0$$

where $\mathcal{G}$ is Gaussian signal term

$$\mathcal{G}(x_i, \sigma_M, M_0) = \frac{1}{\sqrt{2\pi}\sigma_M} e^{-0.5\left(\frac{x_i - M_0}{\sigma_M}\right)^2}.$$

The mass resolution was floating. A projection of the fit function on binned $M(J/\psi\Xi)$ spectrum is presented in Figure 25. Fit resulted in a $\Xi_b$ yield of $20.1 \pm 4.6$ events at a mass of $(5,794 \pm 3.5(\text{stat}))$ MeV/c$^2$. The Gaussian sigma $\sigma_M = (14.8 \pm 2.5(\text{stat}))$ MeV/c$^2$.

The actual mass measurement will be performed using full 5-track vertex fit and is described in the note [17].

#### 5.10.1 Fit systematics

Systematic uncertainties on fit parameters were estimated by running series of toy experiments. In each experiment the total number of events seen in the data in the mass range [5.25,6.5], which is 25, were drawn according to the PDF described above. The PDF parameters were Gaussian

| | Cut | Value |
|---|---|---|
| muon tracks | $N(r-\phi)$ SVX | $> 2$ |
| | $p_T(\mu)$ [GeV/c] | $\geq 1.5$ |
| | $E_{EM}$ | $< 4.$ GeV |
| | $E_{HAD}$ | $< 8.$ GeV |
| | Muon Type | no cut |
| | $\chi^2_x$ for CMU, CMX | $\leq 9$ |
| $J/\psi$ | mass [GeV/c$^2$] | $\vert m(\mu\mu) - M(J/\psi)\vert < 0.08$ |
| | 2-track fit | require success (fit.status=0) |
| proton track | `defTrack` | |
| pion tracks | `defTrack` | |
| $\Lambda^0$ | $\vert\Delta z(p,\pi)\vert$ [cm] | $< 5$ |
| | $L_{xy}$ [cm] | $>= 1$ |
| | 2-track fit $\chi^2(2D)$ | $\leq 49$ |
| | mass [GeV/c$^2$] | $\vert m(p\pi) - M(\Lambda)\vert < 0.01$ |
| | | $p_T(p) > p_T(\pi)$ |
| | pointing angle | $\cos(\alpha) > 0.5$ |
| $\Xi$ | 3-track fit | require success (fit.status=0) |
| | 1-track point. constrain $\Lambda$ vertex to $\Xi$ vertex | |
| | mass [GeV/c$^2$] | $\vert m(\Lambda\pi) - M(\Xi)\vert < 0.01$ |
| | $\Lambda$ displacement in $x-y$ plane [cm] | $R(\Xi)_{vtx} < R(\Lambda)_{vtx} + 1$ |
| | mass constrain $\Xi$ | |
| | mass constrain $\Lambda$ | |
| $\Xi$ track | $N(r-\phi)$ SVX | $> 1$ |
| | $\vert d_0(\Xi)\vert$ [cm] | $\leq 0.1$ |
| $\Xi_b$ | 3-track fit | |
| | mass constrain $J/\psi$ | |

Table 10: Complete list of pre-selection variables and cut values on $J/\psi\Xi$ candidates

| Selection variable | Optimization A | Optimization B |
|---|---|---|
| $p_T(\Xi)$ [GeV/c] | $> 1.7$ | $> 2.5$ |
| $p_T(J/\psi\Xi)$ [GeV/c] | $> 5.$ | $> 6.$ |
| $ct(J/\psi\Xi)$ [cm] | $> 0.008$ | $> 0.01$ |
| $\delta[ct(J/\psi\Xi)]$ [cm] | $< 0.003$ | $< 0.0025$ |
| Pointing angle | $< 0.4$ radians | $< 0.3$ radians |
| $prob(\chi^2(3D))$ | $> 10^{-3}$ | $> 10^{-2}$ |
| $\|d_0(\Xi)\|$ (w.r.t sec vtx.) [cm] | $< 0.01$ | $< 0.008$ |
| $\|d_0(\Xi)_{sig}\|$ (w.r.t. p.v.) | $> 2.5\sigma$ | $> 3.0\sigma$ |
| $\|d_0(J/\psi\Xi)\|$ [cm] | $< 0.0075$ | $< 0.006$ |

Table 11: Selection variables and requirements for Optimization A and Optimization B used to select $\Xi_b \rightarrow J/\psi\Xi$

distributed around their nominal values. The data corresponding to each experiment were fit with the same fit with free parameters. The systematic error is measured by difference between true parameter value and the value obtained from the fit. The distributions of these differences obtained after running 30,000 pseudo-experiments are shown in Figure 26. Table 12 summarized the findings

| Fit parameter | shift |
|---|---|
| yield | $-2.7 \pm 0.03$ |
| Mass | $0.03 \pm 0.03$ MeV/c$^2$ |
| $\sigma_M$ | $-0.62 \pm 0.02$ MeV/c$^2$ |
| constant | $-3.1 \pm 0.3$ |
| slope | $0.031 \pm 0.043$ |

Table 12: Summary if systematic uncertainties on mass fit parameters

Fit biases are investigatied by studying pulls of the fitted parameters. The results are shown in Figure 27.

#### 5.10.2 Mass systematics

Evaluation of systematic uncertainty of mass measurement relies on the stuides that have been performed for the other B hadron species [14]. We compared event-by-event mass differences between events in the Andreas Korn work (which is a subset of our data corresponding to $220pb^{-1}$). The mass difference is shown in Figure 28. The agreement is good with the mean value of $(-0.6 \pm 0.2)$ MeV/c$^2$. Uncertainty due to tracking momentum scale is $\pm 0.4$ MeV/c$^2$, PDG masses $\pm 0.14$ MeV/c$^2$.

The rest of the systematic uncertainty is attributed to the knowledge of the detector resolution and varying fit modes and fit ranges. E.g. if double Gaussians are used to describe the signal, using the values for $\sigma$ obtained from Monte Carlo (See Table 8) gives the value of mass $5,795.0 \pm 3.9$ MeV/c$^2$. The deviation of $\pm 2.0$ MeV/c$^2$ is assigned as fit procesure systematic uncertainty.

Table 13 summarizes mass fit uncertainties. The final number for the $\Xi_b^-$ mass is:

$$M(\Xi_b^-) = (5,794.0 \pm 3.5 \pm 1.8)\ \text{MeV/c}^2$$

| source | uncertainty [MeV/c$^2$] |
|---|---|
| Fit bias | $0.03 \pm 0.03$ |
| Mass calibration | $-0.6 \pm 0.2$ |
| Momentum scale | $\pm 0.4$ |
| PDG masses | $\pm 0.14$ |
| Fit model/resolution | $\pm 1.5$ |
| Total | $\pm 1.8$ |

Table 13: Summary of mass systematic uncertainties

### 5.11 Significance estimate

Following recipe developed in [15] we calculate p-value as probability of $N_{total}$ events in a large mass range to produce $N_{signal}$ events in the narrow region of interest. We use $N_{total} = 27$ events in the mass range [5.6-6.5] GeV/c$^2$. Lower boundary chosen to be approximately mass of the $\Xi_b$ minus mass of the pion to guarantee that we are operating in the region where background is mostly flat. The signal region is chosen to be $(5,794 \pm 0.03)$ GeV/c$^2$ that is 60 MeV/c$^2$ wide. In this region there are $N_{signal} = 20$ events. The probability of 27 events from the mass range of width 0.9 GeV/c$^2$to produce 20 events in the region of 60 MeV/c$^2$assuming flat event distribution is $3.3 \cdot 10^{-6}$ which corresponds to Gaussian significance of more than $8\sigma$.

## 6 Search for $\Xi_b$ in TTT data

The displaced track trigger dataset may provide an exciting opportunity to discover a neutral isospin partner of $\Xi_b^-$ in the decay channel $\Xi_b^0 \to \Xi_c^+ \pi^-$. Also another bottom-strange baryon $\Omega_b$ could be searched for in the decay chain $\Omega_b D^0 \Xi^-$.

The TTT sample is expected to contain high statistics signals of decays involving $\Xi$ in the final state. Measurements of masses of such known states as $\Xi(1530)^0$, $\Xi_c^+$ and $\Xi_c^0$ allows to study systematic effects caused by our $\Xi$-tracking.

### 6.1 Mass measurements of states involving $\Xi$ as decay product

We start with the mass measuerement studies performed in 1.2 $fb^{-1}$ of data.

#### 6.1.1 Reconstruction of $\Xi(1530)^0 \to \Xi^- \pi^+$

We should stress that $\Xi$ hyperons do not produce two tracks satisfying SVT trigger criteria. Therefore, in the SVT data, we are looking for $\Xi\pi^+$ candidates that are not required to satisfye the SVT trigger. As the SVT triggers predominantly on the tracks left by the particles produced in decays of long lived $c$- and $b$- hadrons, the source of pentaquark canduidates is the production in fragmentation of non leading quarks.

The invariant mass of $\Xi\pi^+$ pairs is represented by points with error bars in Figure 29. The mooth curve is the projection of the unbinned likelihood. All fit paramaters were free except natural widths of $\Xi(1530)$ which was constrained to world average value of $(9.1 \pm 0.5)$ MeV/c$^2$.

We used CERN MINUIT package to minimize:

$$
\begin{aligned}
F &= -2\ln\mathcal{L} \\
-\ln\mathcal{L} &= \mathcal{F}(\vec{\alpha}) - \sum_i^N \ln f(x_i,\vec{\alpha}) + \frac{1}{2}\left(\frac{\Gamma-9.1}{0.5}\right)^2 \\
\mathcal{F}(\vec{\alpha}) &= \int_a^b f(x,\vec{\alpha})dx
\end{aligned}
\tag{1}
$$

where, $a$ and $b$ are integration limits (1.4 and 2.2 GeV/c$^2$ respectively) and index $i$ is running over the number of candidates $N$. The function $f(x,\vec{\alpha})$ is the sum of background term:

$$B(m,\vec{\alpha}) = (0.5\cdot(|m-(M_\pi+M_\Xi)|+m-(M_\pi+M_\Xi)))^{\alpha_0}\cdot\left(\sum_{i=0}^{3}\alpha_{i+1}\cdot(m-M)^i\right) \tag{2}$$

and signal terms, describing $\Xi(1530)$. The signal term is represented by Breit-Wigner resonance function convoluted with the Gaussian mass resolution function:

$$S(m) = N(BW\otimes G(m,\Gamma,\sigma,M))/I \tag{3}$$

where $I$ is the integral:

$$I = \int_{M-10\bar{\sigma}}^{M+10\bar{\sigma}} BW\otimes G(m,\Gamma,\sigma,M)dm \tag{4}$$

where $\bar{\sigma} = \sqrt{\sigma^2+0.25\Gamma^2}$. The limits $\pm 10\bar{\sigma}$ are somewhat arbitrary, corresponding to 94% of integral of unsmeared Breit-Wigner:

$$\int_{M-10\bar{\sigma}}^{M+10\bar{\sigma}} BW(m,\Gamma,M)dm = \frac{1}{\pi}\arctan\left(\frac{m-M}{0.5\Gamma}\right)\Bigg|_{M-10\bar{\sigma}}^{M+10\bar{\sigma}} \tag{5}$$

### 6.1.2 Reconstruction of $\Xi_c^0$ and $\Xi_c^+$

Unlike $\Xi(1530)^0$ the members of isosping doublet $\Xi_c^0$ and $\Xi_c^+$ decay weakly to $\Xi^-\pi^+$ and $\Xi^-\pi^+\pi^+$ respectively producing displaced decay vertices.

$$
\begin{array}{rlrl}
\Xi_c^0 \to & \Xi^- + \pi^+ & ,\ \Xi_c^+ \to & \Xi^- + \pi^+\pi^+ \\
\hookrightarrow & \Lambda\pi^- & \hookrightarrow & \Lambda\pi^- \\
 & ct = 29\mu m & & ct = 132\mu m
\end{array}
$$

Therefore the requirement of the decay pion to be matched with SVT trigger primitive is a must to control combinatorial background. Other cuts inclde $L_{xy}$, $p_T$, $ct$, $\delta ct$ and fit probability. The distributions of these variables are shown in Figures 31 for $\Xi_c^0$ and and in Figures 32 for $\Xi_c^+$. The cuts chosen are listed in Table 14. Table 15 summarizes mass measurements for $\Xi(1530)$ , $\Xi_c^0$ and $\Xi_c^+$ states.

Figure 35 shows graph of Q(CDF)-Q(PDG) vs Q(CDF). A linear fit is superimposed. The dependence is given by equation:

$$\delta m = (-8.05\pm 6.49)\cdot 10^{-4}\cdot Q[\mathrm{MeV/c^2}] - (0.58\pm 0.68)[\mathrm{MeV/c^2}]$$

For a Q-value in the decay $\Xi_b \to J/\psi\Xi$, assuming mass of $\Xi_b$ is 5,794 MeV/c$^2$ we can extrapolate the mass uncertainty to be:

$$\delta m = -1.69\pm 1.54\ \mathrm{MeV/c^2}$$

We conclude that there is no significant mass bias introduced by $\Xi$ tracking and selection.

| Selection variable | cut value |
|---|---|
| $p_T(\Xi_c)$ | $> 4.$ |
| $Lxy(\Xi_c)$ | $> 0.02$ |
| $ct(\Xi_c)$ | $> 0.025$ |
| $\delta(ct(\Xi_c))$ | $< 0.004$ |
| $prob(\chi^2(3D))$ | $> 10^{-4}$ |

Table 14: Cuts applied to $\Xi_c^0$ and $\Xi_c^+$ candidates.

| State | measured mass [MeV/c$^2$] | PDG value [MeV/c$^2$] | difference [MeV/c$^2$] |
|---|---|---|---|
| $\Xi(1530)$ | $1,532.23 \pm 0.08$ | $1,531.78 \pm 0.34$ | $0.45 \pm 0.35$ |
| $\Xi_c^0$ | $2,470.5 \pm 0.6$ | $2,471.09^{+0.35}_{-1.00}$ | $-0.59^{+0.69}_{-1.17}$ |
| $\Xi_c^+$ | $2,467.6 \pm 0.3$ | $2,467.6^{+0.4}_{-1.0}$ | $0.00^{+0.5}_{-1.0}$ |

Table 15: Cuts applied to $\Xi_c^0$ and $\Xi_c^+$ candidates.

# 7 Conclusion

Using selection criteria were obtained in unbiased manner on a control sample of $B^+ \to J/\psi K^+$ decays following verbatim the strategy of $B_c$ search by Fermilab group [4] a significant ($> 8.5\sigma$) is observed at a mass $M(\Xi_b^-) = (5,794.0 \pm 3.5 \pm 1.8)$ MeV/c$^2$ in $J/\psi\Xi$ invariant mass spectrum where $\Xi$ track is reconstructed in SVX. The data sample used comprise integrated luminosity of about 1.9 fb$^{-1}$.

## References


[1] E.A. Gerchtein, D.O. Litvintsev, P.T. Lukens "Tracking of Hyperons in SVX detector" CDF/PUB/TRACKING/PUBLIC/6527

[2] E.A. Gerchtein, D.O. Litvintsev, P.T. Lukens "A Search for Exotic S=-2 Baryons Decaying to $\Xi^{\pm}\pi^{\pm}$" CDF/ANAL/BOTTOM/CDFR/6855

[3] K. Bloom, W.-M. Yao, ""Outside-In" Silicon Tracking at CDF", CDF/DOC/TRACKING/CDFR/5991
H. Wenzel, "Tracking in the SVX", CDF/DOC/SEC_VTX/CDFR/1790

[4] P. Lukens, S. Tkaczyk, W. Wester "Search for the Exclusive $B_c \to J/\psi\pi$ Decay" CDF/ANAL/BOTTOM/CDFR/7572; P. Lukens, S. Tkaczyk, W. Wester "Observation of the $B_c \to J/\psi\pi$ Decay" CDF/ANAL/BOTTOM/CDFR/7881;

[5] Mario Campanelli, Elena Gerchtein CDF Note Number: CDF/PHYS/BOTTOM//6905

[6] Update on the measurement of $\mathcal{B}(B^+ \to J/\psi\pi^+)/\mathcal{B}(B^+ \to J/\psi K^+)$ by Jaison Lee Ilsung Cho Intae Yu Ting Miao

[7] J. G. Korner, M. Kramer and D. Pirjol, Prog. Part. Nucl. Phys. **33**, 787 (1994)

[8] A. De Rujula, H. Georgi and S. L. Glashow, Phys. Rev. D **12**, 147 (1975).

[9] C. Albertus, E. Hernandez and J. Nieves, arXiv:hep-ph/0408065.

[10] N. Mathur, R. Lewis and R. M. Woloshyn, Phys. Rev. D **66**, 014502 (2002) [arXiv:hep-ph/0203253].

[11] Particle Data Group, K. Hagiwara *et al.*, Phys. Rev. **D 66**, 2002

[12] I. Dunietz, Z. Phys. C **56**, 129 (1992).

[13] A. Abulencia *et al.* [CDF Collaboration], arXiv:hep-ex/0609021.

[14] D. Acosta *et al.* [CDF Collaboration], Phys. Rev. Lett. **96**, 202001 (2006) [arXiv:hep-ex/0508022]. (CDF/ANAL/BOTTOM/CDFR/6963)

[15] P. Lukens "Evidence for $Xi_b \to J/\psi\Xi$" CDF/ANAL/BOTTOM/CDFR/8650

[16] CDF/ANAL/BOTTOM/CDFR/3458

[17] Observation of Bottom-Strange Baryon $\Xi_b$ and measurement of its mass. D.Litvintsev, P.Lukens.

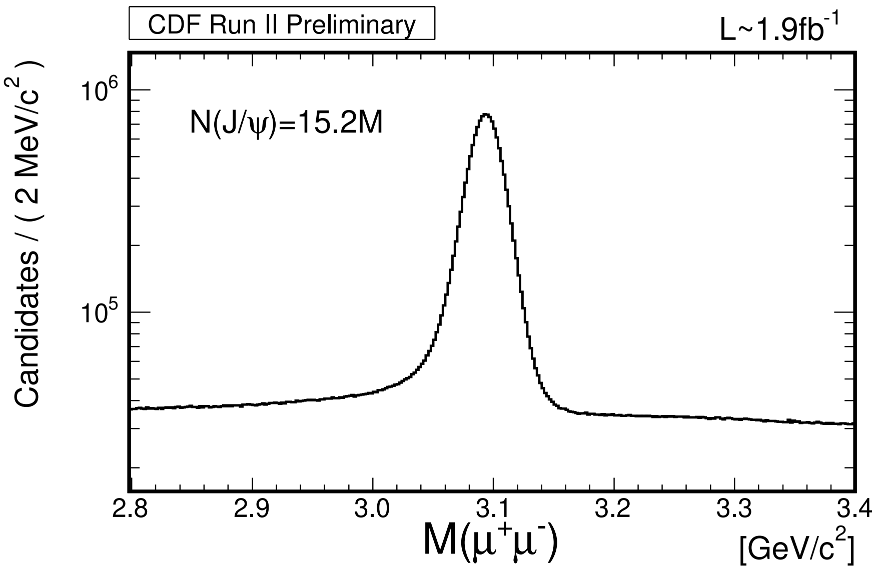


Figure 2: Invariant mass of di-muon candidates in 1.9 fb$^{-1}$. The event yield is calculated using sideband subtraction. See text for details.

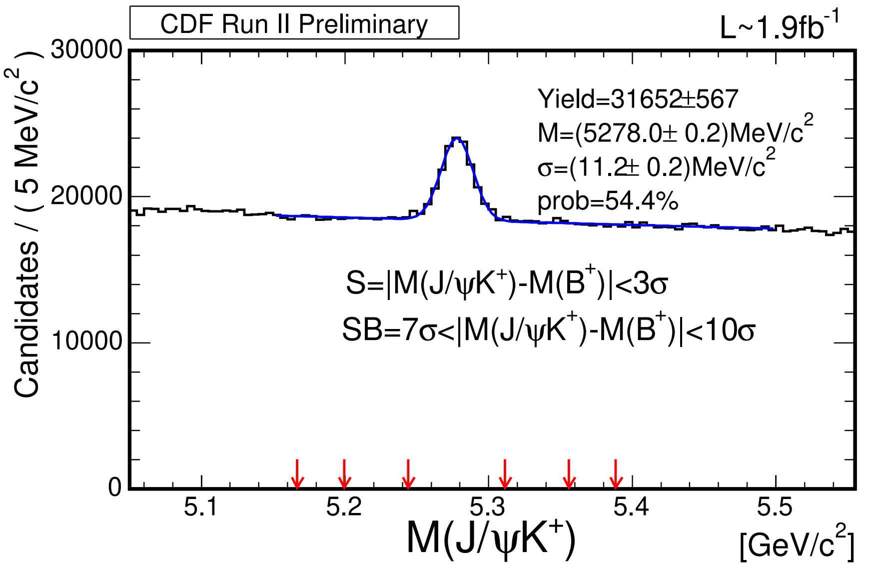


Figure 3: Invariant mass of $J/\psi K^+$ candidates satisfying loose pre-selection criteria. Arrows mark boundaries of signal and sideband intervals.

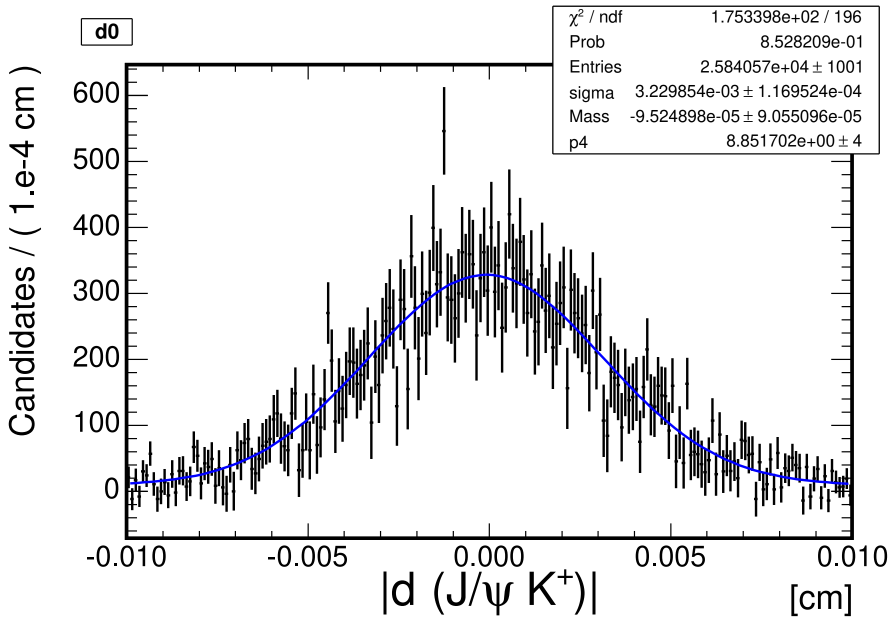


Figure 4: Sideband subtracted distribution of $B^+$ signed impact parameter $d_0(J/\psi K^+)$. A fit to a signle Gaussian is superimposed (Data Sample isapproxmately 1.35 $fb^{-1}$). This plot is based on 1.6 $fb{-}1$ of data.

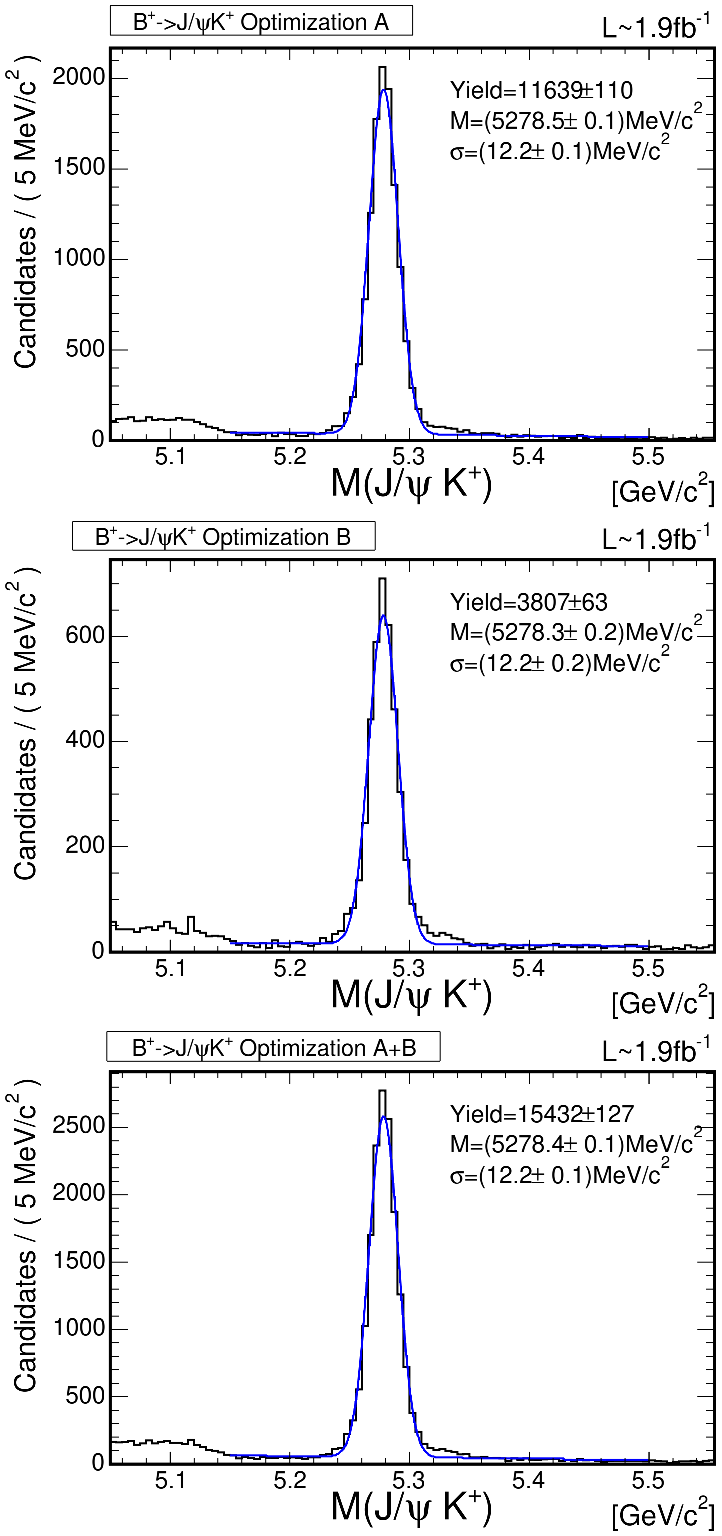


Figure 5: $J/\psi K^+$ invariant mass spectra after optimized cuts are applied. From top to bottom: Optimization A, Optimization B and the sum of the two.

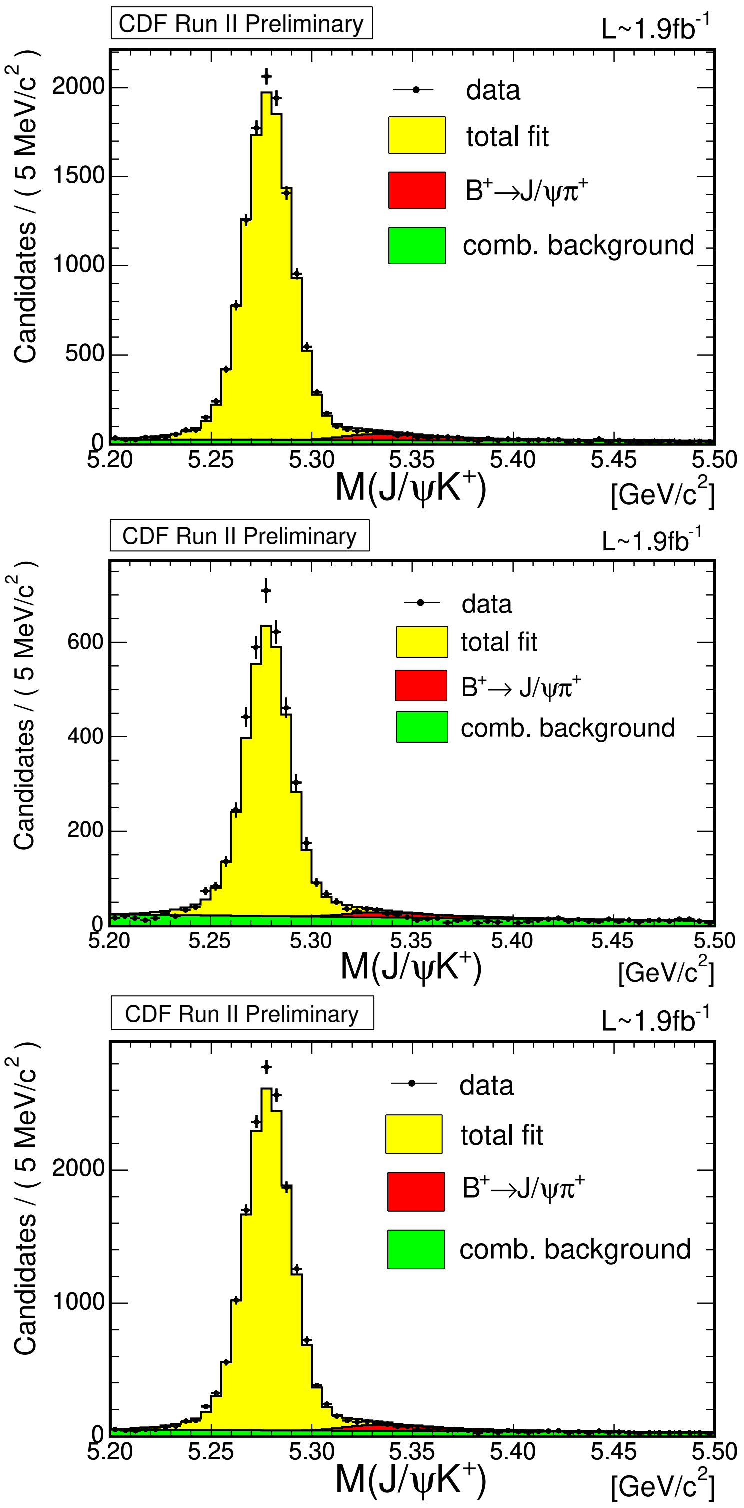


Figure 6: $J/\psi K^+$ invariant mass spectra after optimized cuts are applied. From top to bottom: Optimization A, Optimization B and the sum of the two. Histograms drawn with solid line show result of unbinned log likelihood fit described in the text.

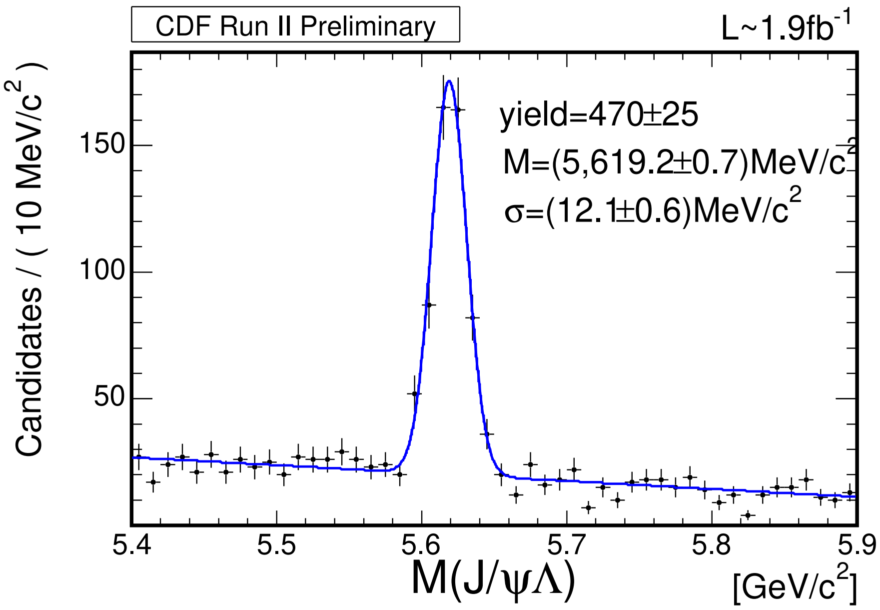


Figure 7: Invariant mass spectrum of $J/\psi\Lambda^0$ combinations after applying cuts close to one blessed for $\Lambda_b$ lifetime paper [13]. The smooth curve shows result of an unbinned maximum log-likelihood fit to the data with single Gaussian and liner background. All parameters in the fit were floating.

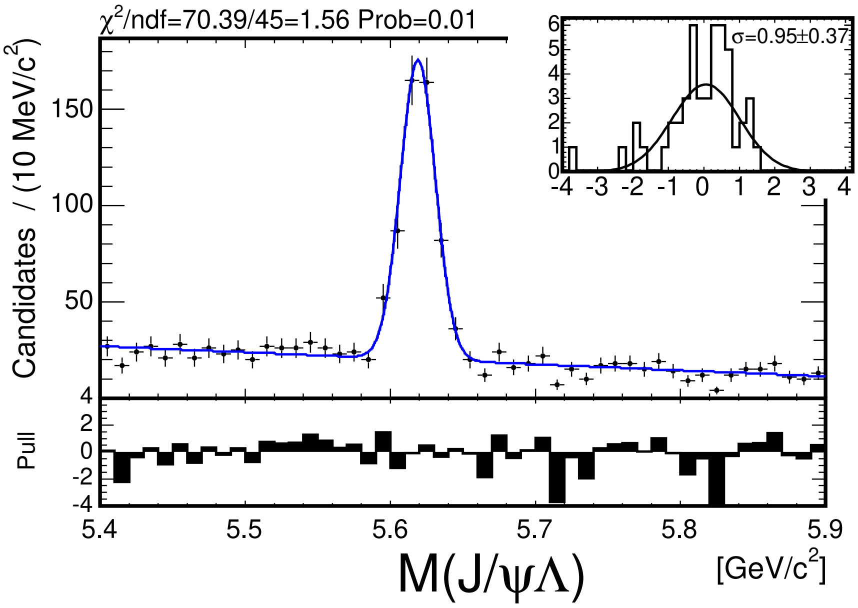


Figure 8: Fit residuals

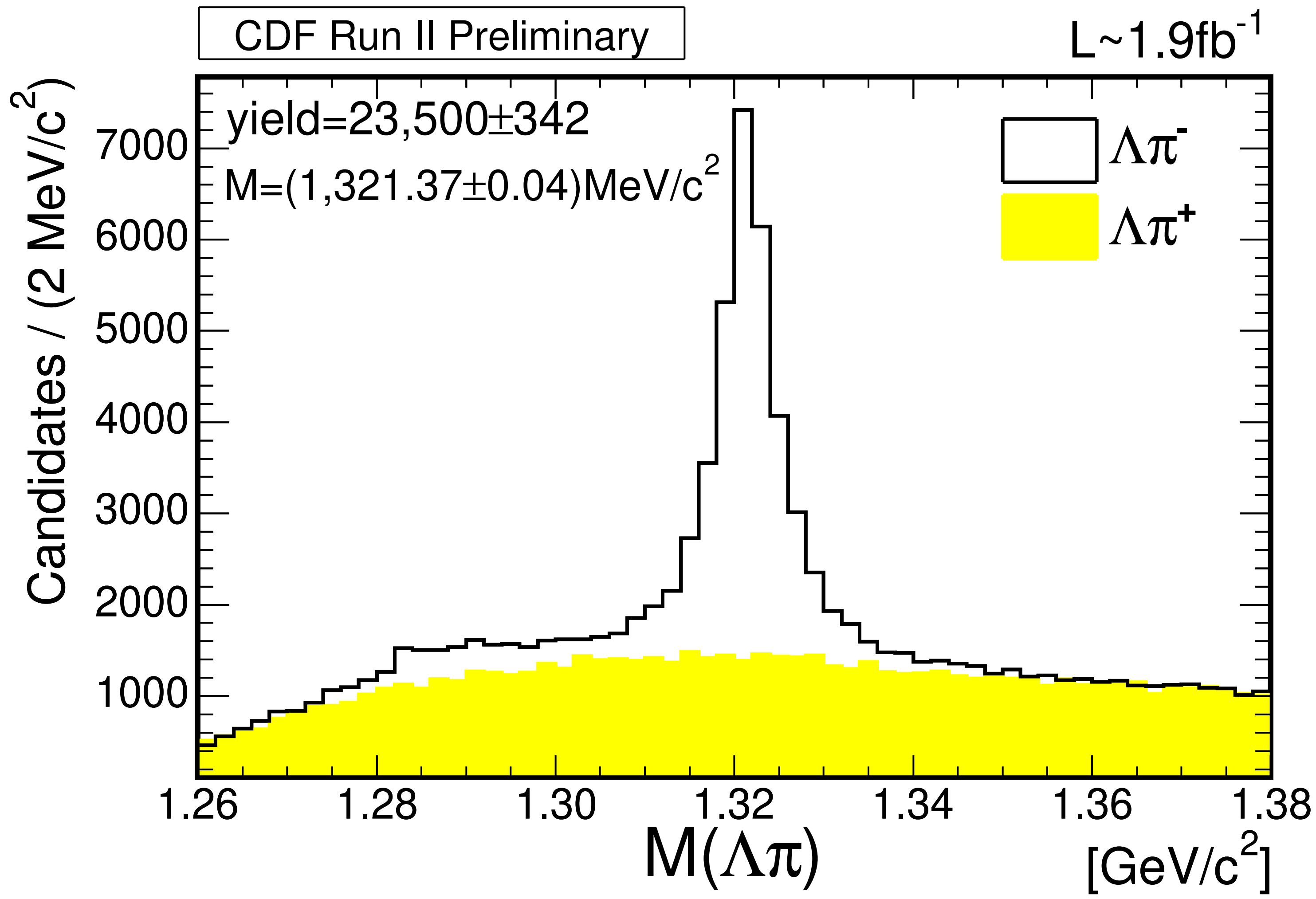


Figure 9: Invariant mass spectrum of $\Lambda\pi$ combinations having associated silicon $\Xi$ track. Shaded histogram show wrong sign combinations $\Lambda\pi^+$. Soft requirement on $|d_0(\Xi)| < 0.1$ cm

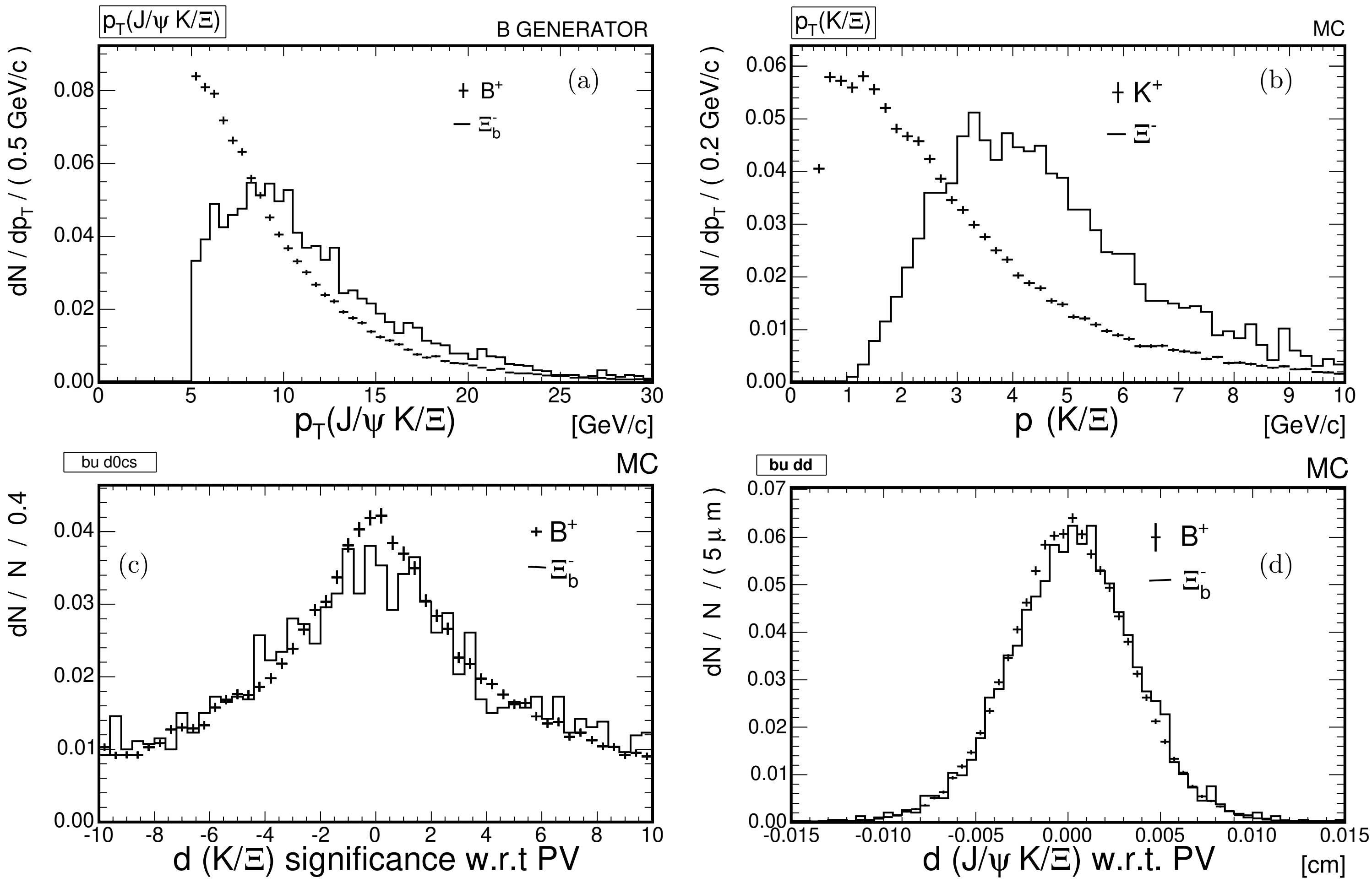


Figure 10: Simulated data. Comparison of selection quantities between $B^+ \to J/\psi K^+$ and $\Xi_b^- \to J/\psi \Xi^-$. (a) $p_T(J/\psi K/\Xi)$. Optimization A cut is $p_T > 5$ GeV/c. Optimization B cut is $p_T > 6$ GeV/c. (b) $p_T(K/\Xi)$. Optimization A cut is $p_T > 1.7$ GeV/c. Optimization B cut is $p_T > 2.5$ GeV/c. (c) $d_0(K/\Xi)$ significance w.r.t. P.V. Optimization A cut is $> 2.5$, Optimization B cut $> 3$. (d) signed impact parameter of $B^+/Xi_b^-$ candidates. Optimization A cut is $< 0.0075$, Optimization B cut $< 0.006$.

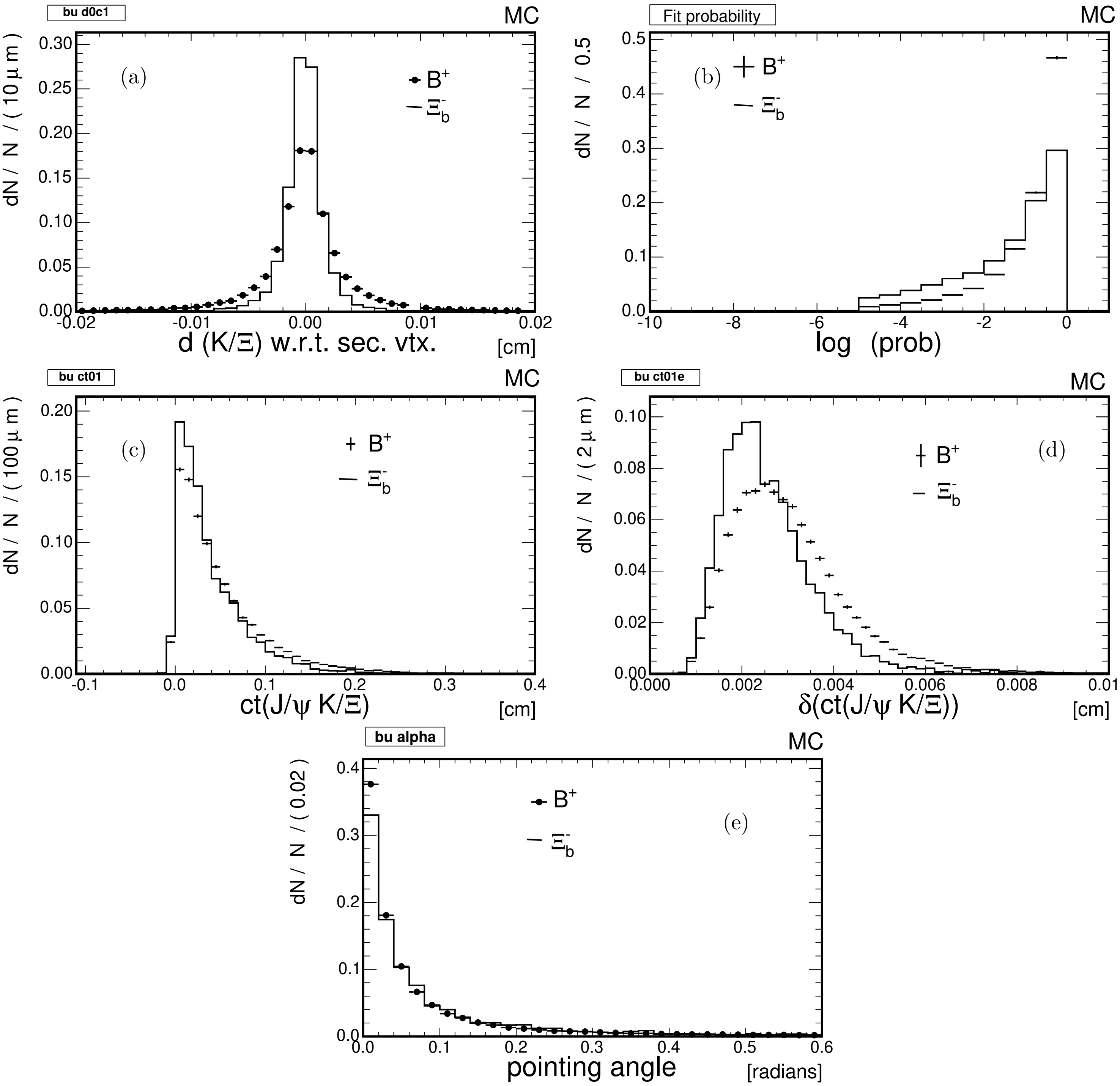


Figure 11: Simulated data. Comparison of selection quantities between $B^+ \rightarrow J/\psi K^+$ and $\Xi_b^- \rightarrow J/\psi \Xi^-$. (a) signed impact parameter of the third track w.r.t. secondary vertex. Optimization A cut is $< 0.01$. Optimization B cut is $< 0.008$. (b) $\log_{10}(prob(\chi^2(3D)))$. Optimization A cut is $> 10^{-3}$. Optimization B cut is $> 10^{-2}$. (c) $ct(J/\psi K/\Xi)$, both particles were generated with identical lifetimes. Optimization A cut is $> 0.008$, Optimization B cut $> 0.01$. (d) $\delta(ct(J/\psi K/\Xi))$. Optimization A cut is $< 0.003$, Optimization B cut $> 0.0025$. (e) pointing angle. Optimization A cut is $< 0.4$, Optimization B cut is $< 0.3$.

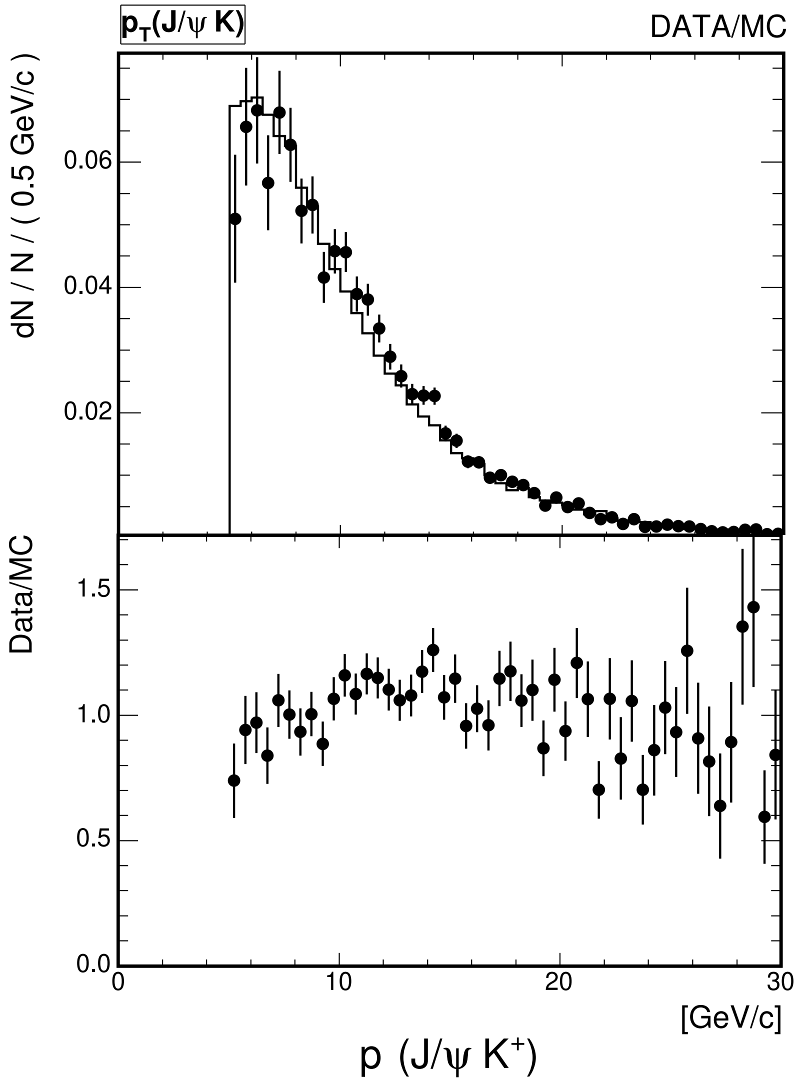


Figure 12: Data/MC comparison of $B^+ \to J/\psi K^+$ candidates. Transverse momentum of $J/\psi K^+$. Points with error bars represent real data obtained by sideband subtraction.

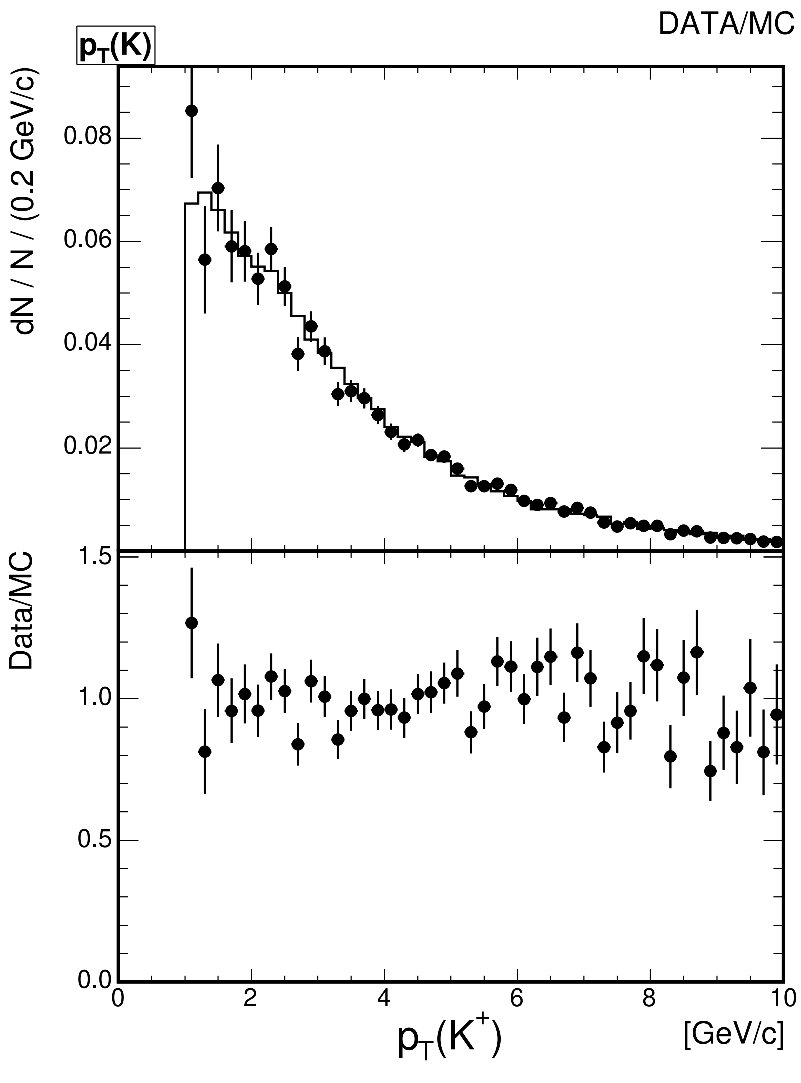


Figure 13: Data/MC comparison of $B^+ \to J/\psi K^+$ candidates. Transverse momentum of $K^+$. Points with error bars represent real data obtained by sideband subtraction.

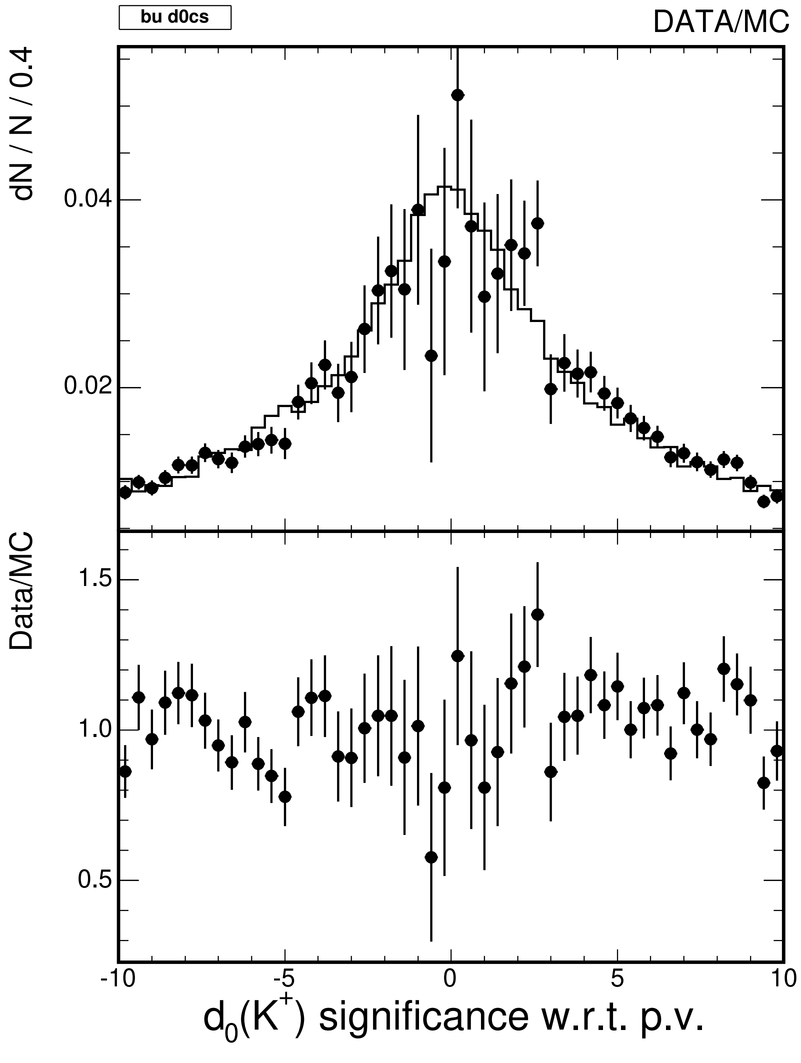


Figure 14: Data/MC comparison of $B^+ \to J/\psi K^+$ candidates. Impact parameter significance of $K^+$ w.r.t. PV. Points with error bars represent real data obtained by sideband subtraction.

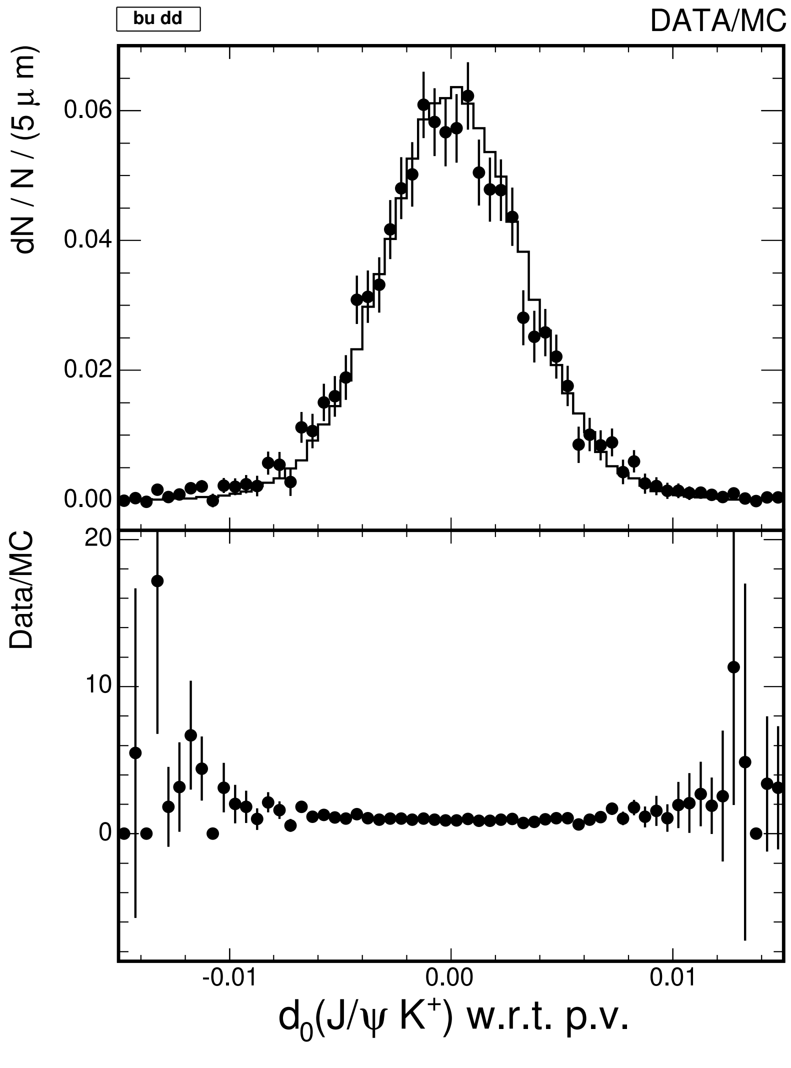


Figure 15: Data/MC comparison of $B^+ \to J/\psi K^+$ candidates. Signed impact parameter of $J/\psi K^+$. Points with error bars represent real data obtained by sideband subtraction.

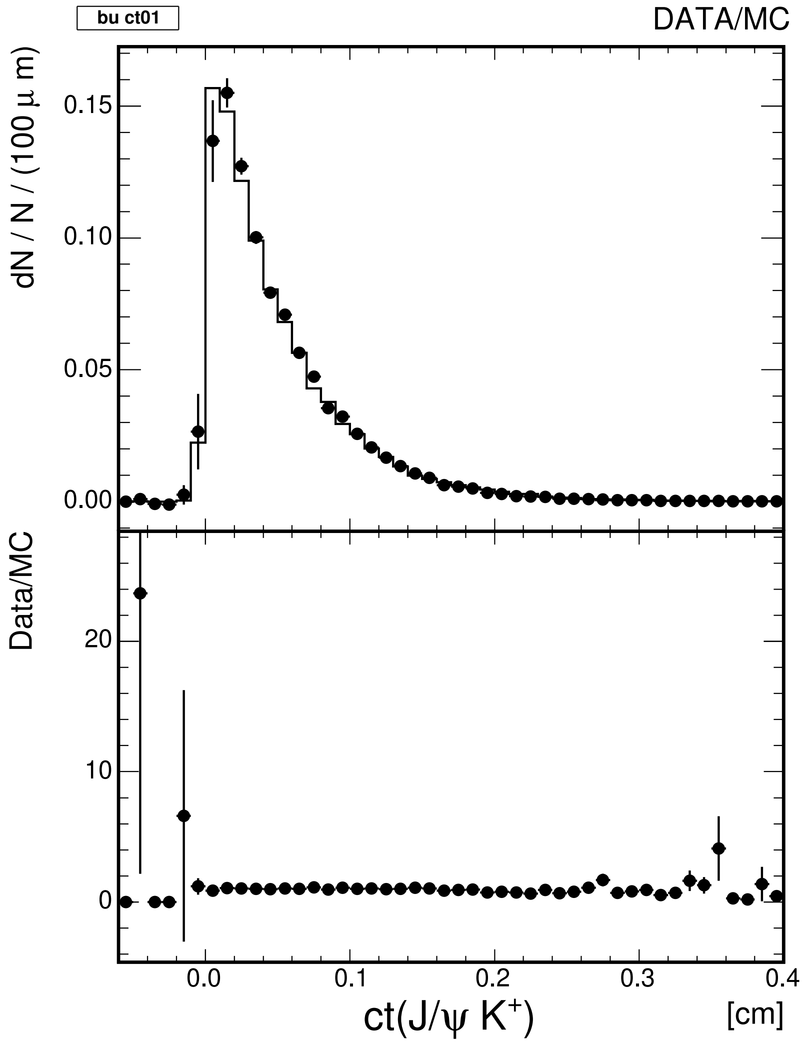


Figure 16: Data/MC comparison of $B^+ \to J/\psi K^+$ candidates. $ct(J/\psi K^+)$. Points with error bars represent real data obtained by sideband subtraction.

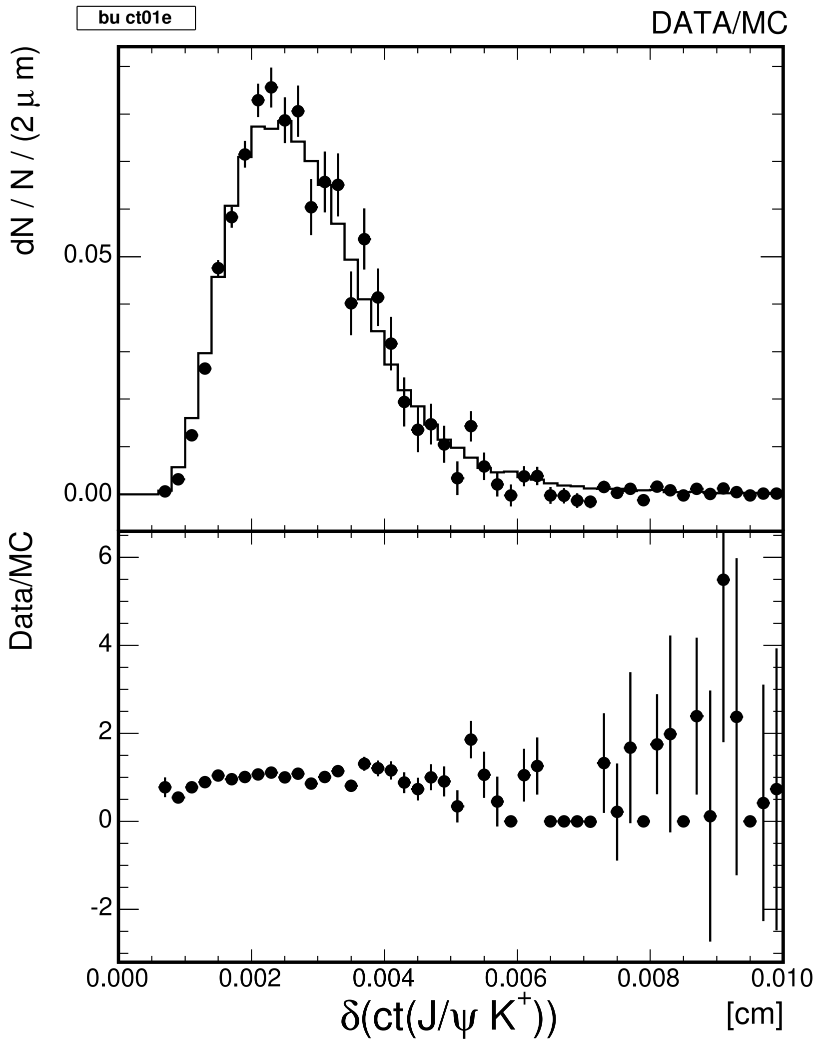


Figure 17: Data/MC comparison of $B^+ \to J/\psi K^+$ candidates. $\delta(ct(J/\psi K^+))$. Points with error bars represent real data obtained by sideband asubtraction.

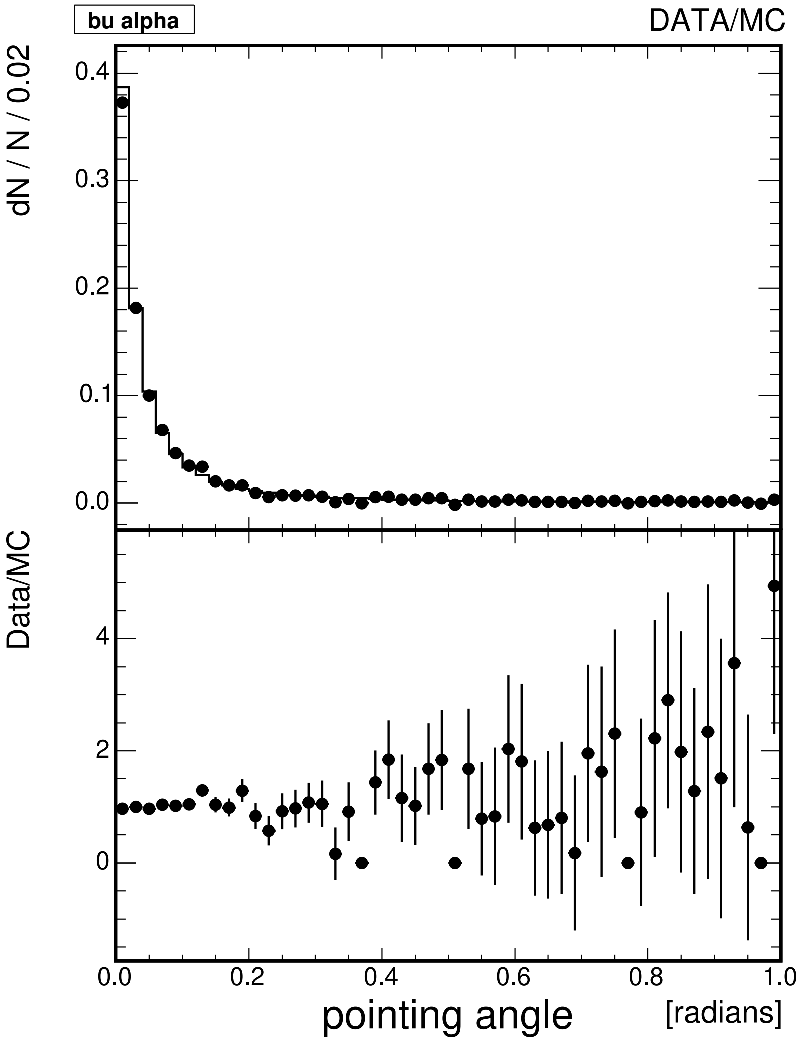


Figure 18: Data/MC comparison of $B^+ \to J/\psi K^+$ candidates. Pointing angle of $J/\psi K^+$ candidates. Points with error bars represent real data obtained by sideband asubtraction.

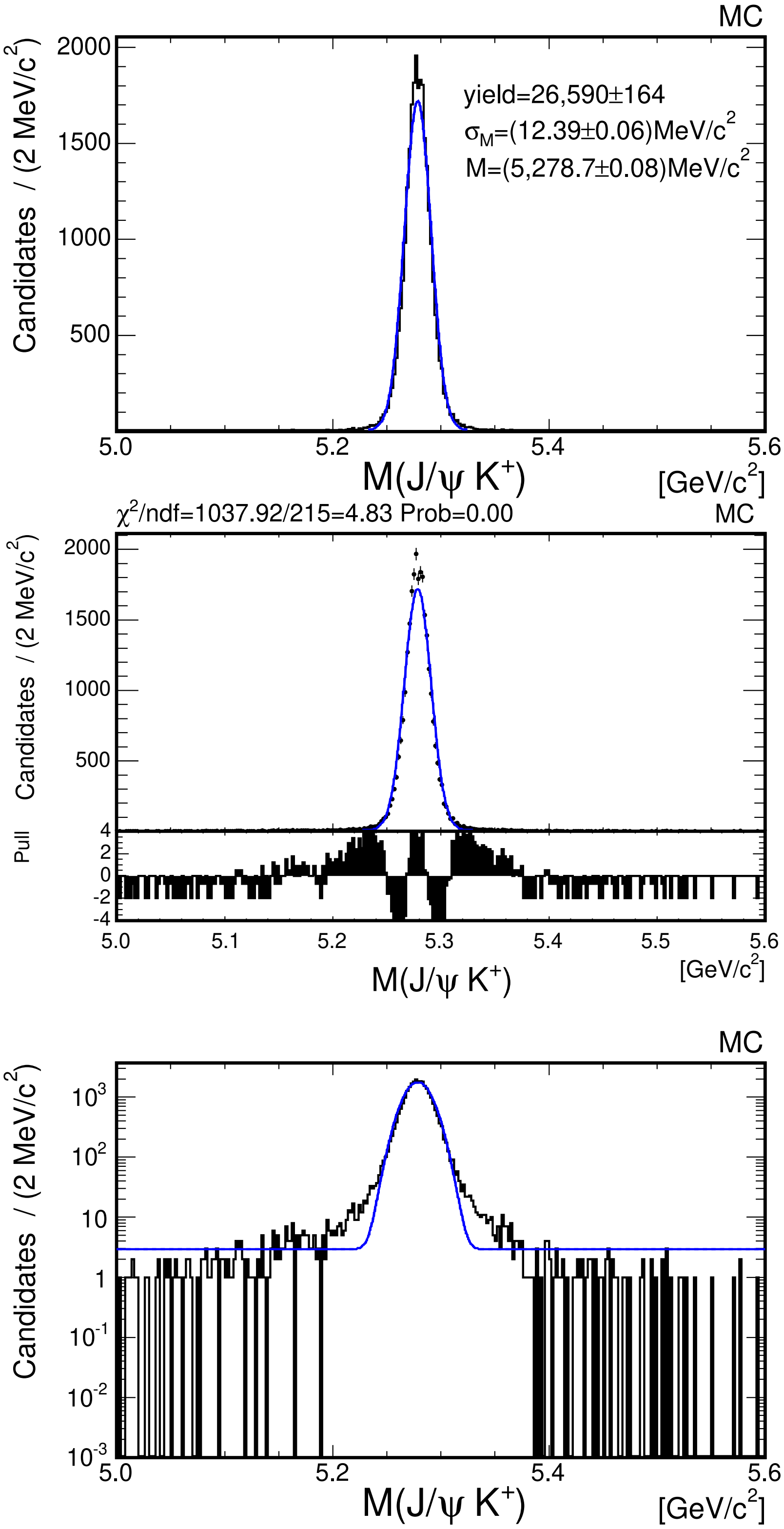


Figure 19: Simulated invariant mass spectra of $B^+ \to J/\psi K^+$ candidates. Top – projection of an unbinned, single Gaussian fit to the simulated data. Center – Fit residuals. Bottom – projection of an unbinned, single Gaussian fit to the simulated data shown in logarithmic scale to reveal fine details of the spectrum.

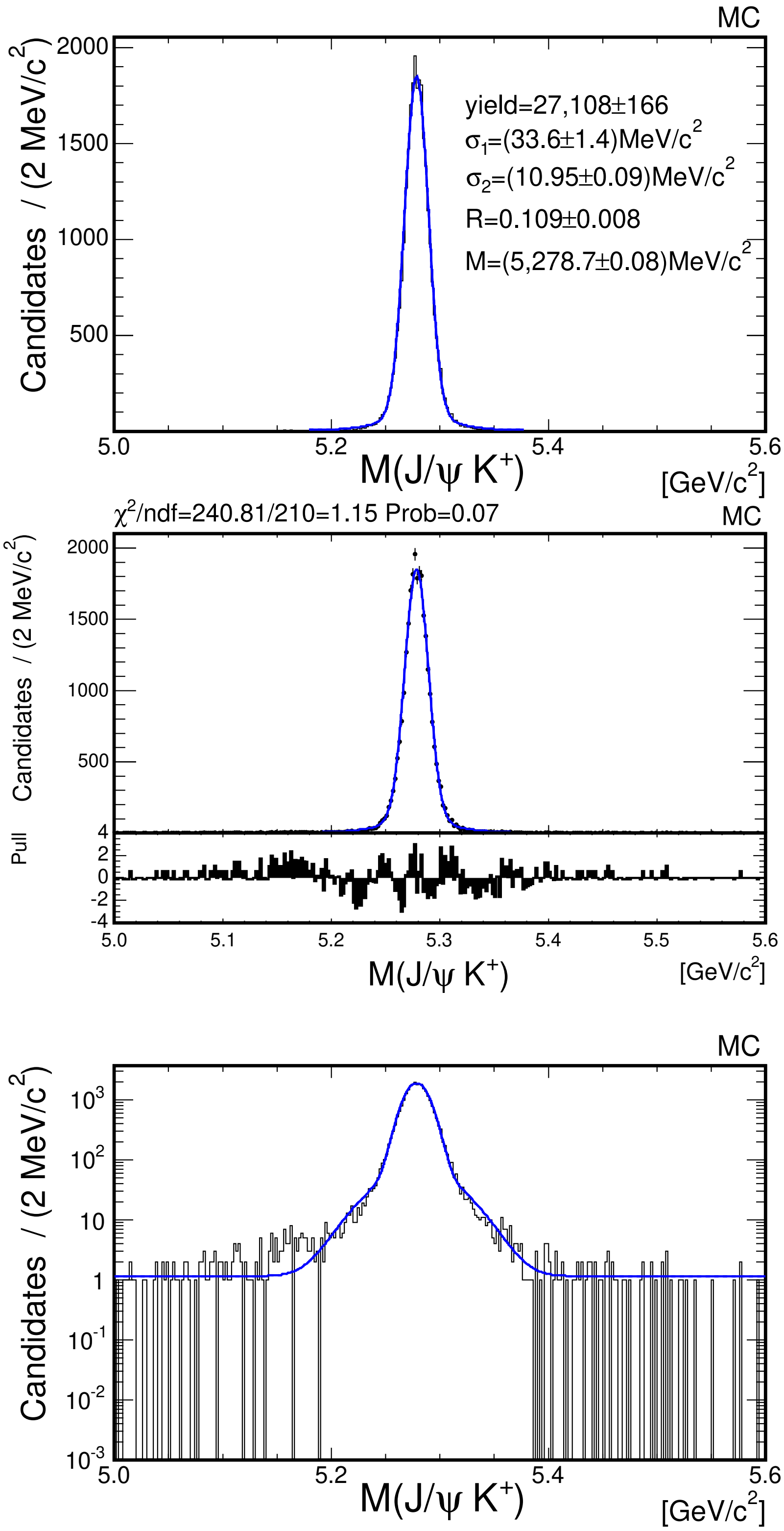


Figure 20: Simulated invariant mass spectra of $B^+ \to J/\psi K^+$ candidates. Top – projection of an unbinned, double Gaussian fit to the simulated data. Center – Fit residuals. Bottom – projection of an unbinned, double Gaussian fit to the simulated data shown in logarithmic scale to reveal fine details of the spectrum.

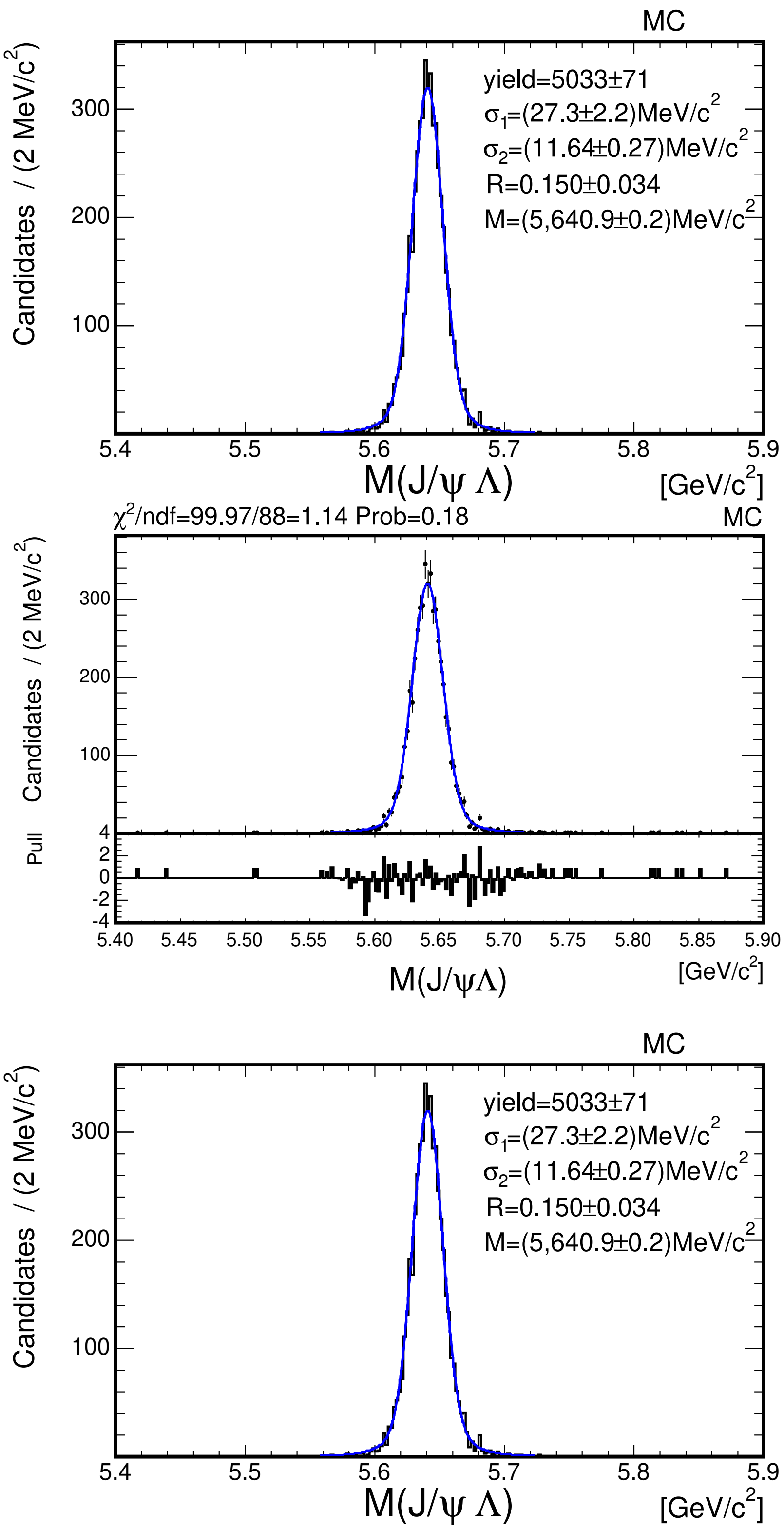


Figure 21: Simulated invariant mass spectra of $\Lambda_b^0 \to J/\psi\Lambda^0$ candidates. Top – projection of an unbinned, double Gaussian fit to the simulated data. Center – Fit residuals. Bottom – projection of an unbinned, double Gaussian fit to the simulated data shown in logarithmic scale to reveal fine details of the spectrum.

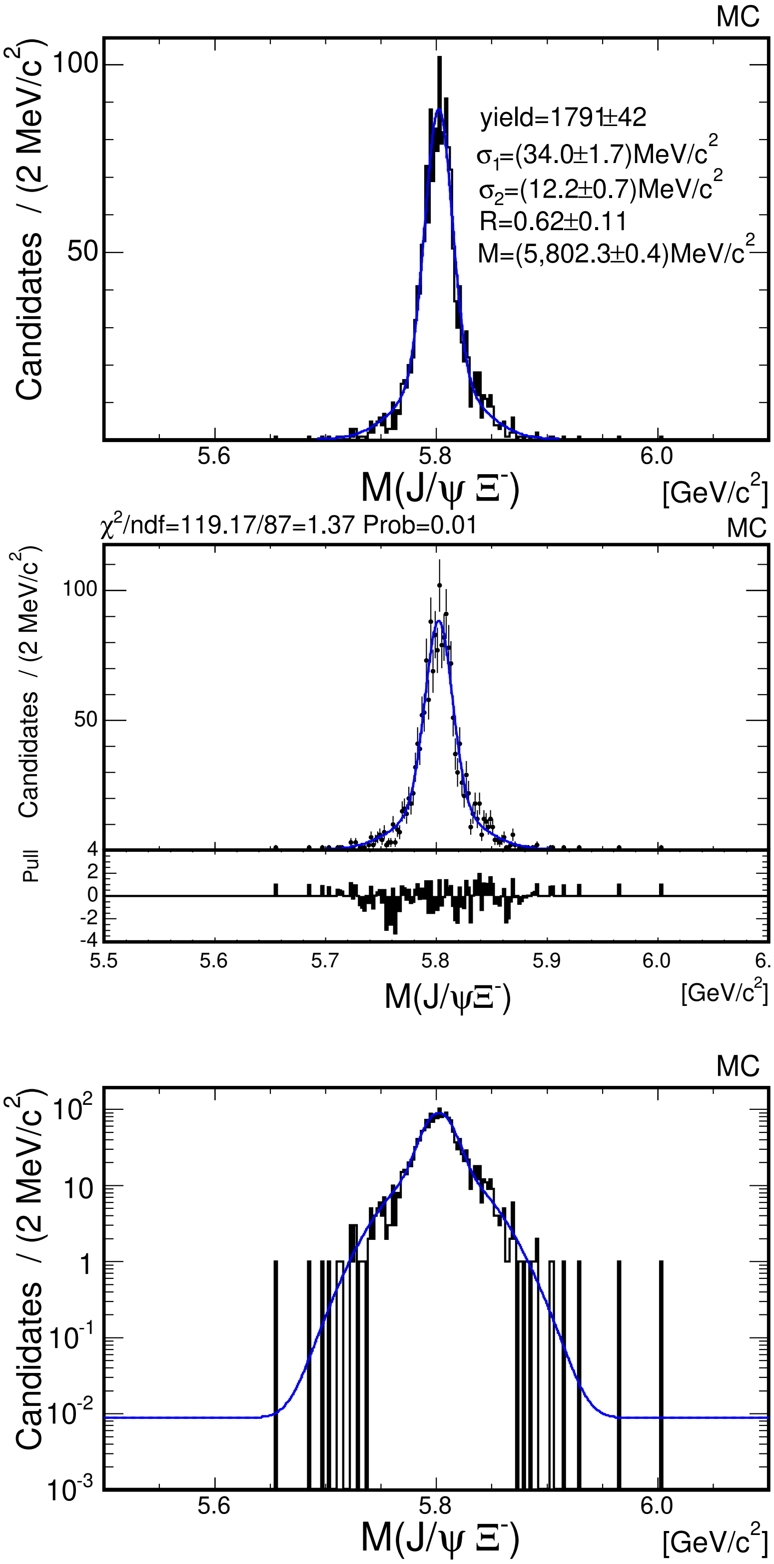


Figure 22: Simulated invariant mass spectra of $B^+ \to J/\psi\Xi^-$ candidates. Top – projection of an unbinned, double Gaussian fit to the simulated data. Center – Fit residuals. Bottom – projection of an unbinned, double Gaussian fit to the simulated data shown in logarithmic scale to reveal fine details of the spectrum.

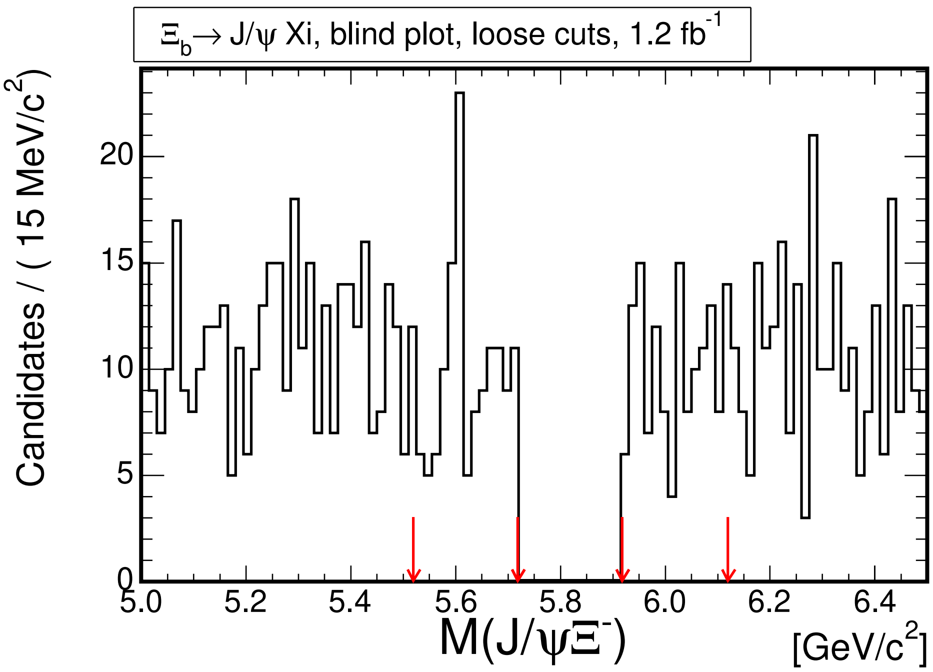


Figure 23: Invariant mass of $J/\psi\Xi$ candidates satisfying loose pre-selection criteria. Arrows mark boundaries of signal and sideband intervals. This is plot corresponds to older, approximately 1.35 $fb^{-1}$ sample.

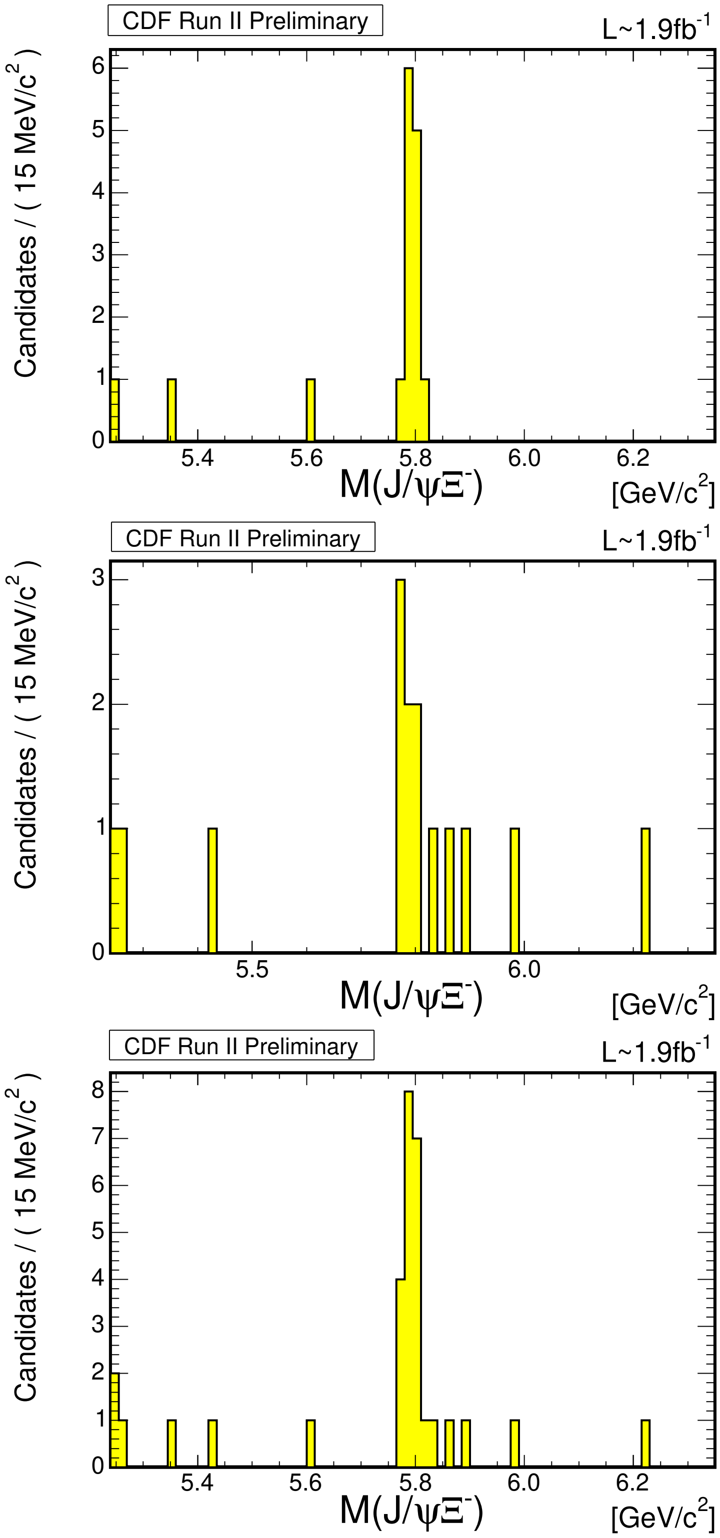


Figure 24: Invariant mass spectra of $J/\psi\Xi$ candidates in $1.9fb^{-1}$. From top to bottom: Optimization A, Optimization B, Optimization A+B.

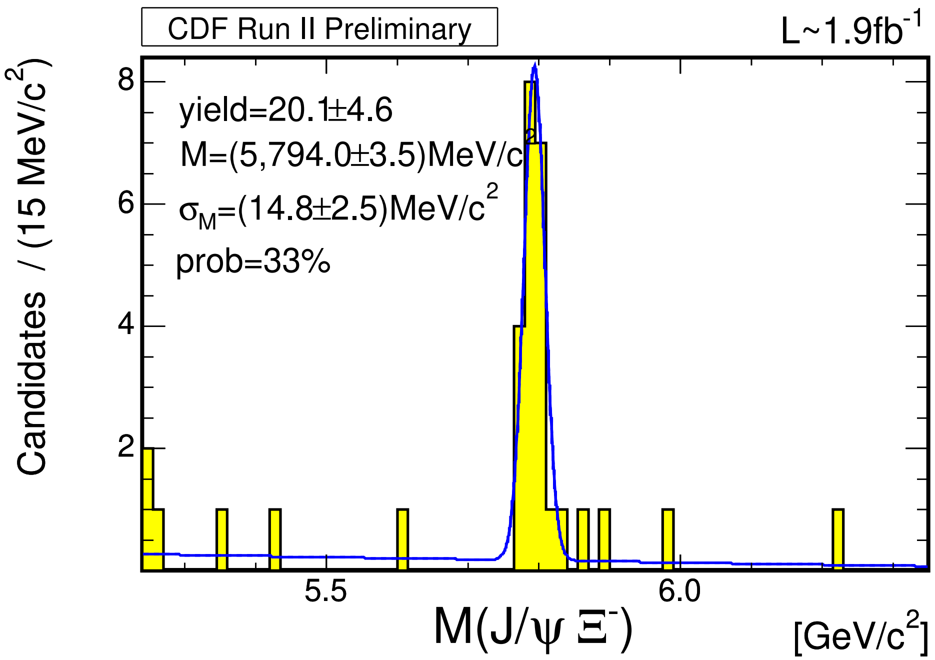


Figure 25: Projection of an unbinned maximum log likelihood fit on the invariant mass spectrum of $\Xi_b \to J/\psi\Xi$ candidates. The same as Figure above, smaller mass window. Fit is done to avoid bumps from $\Xi_b \to J/\psi\Xi X$ decays.

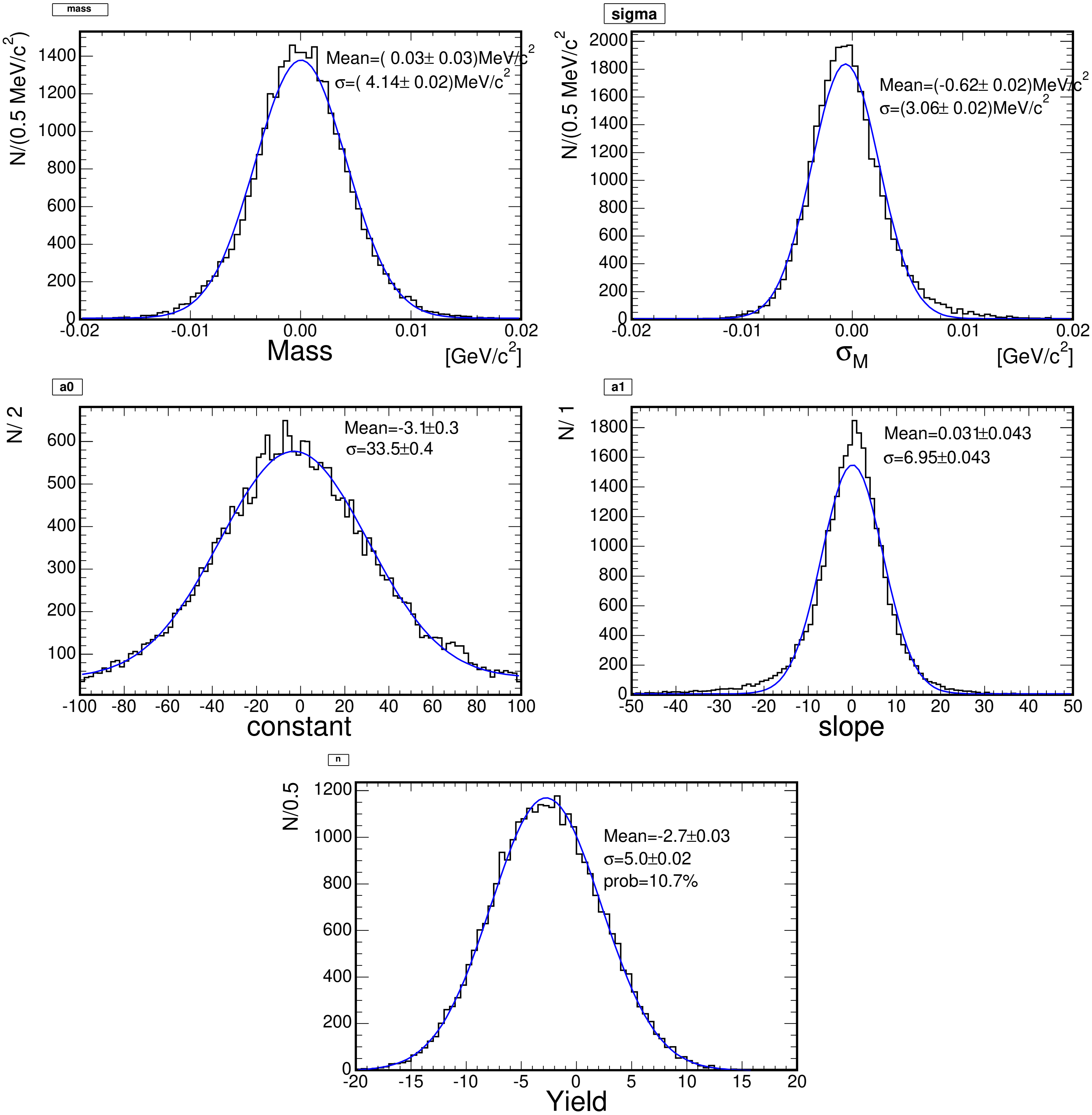


Figure 26: Fit Pulls

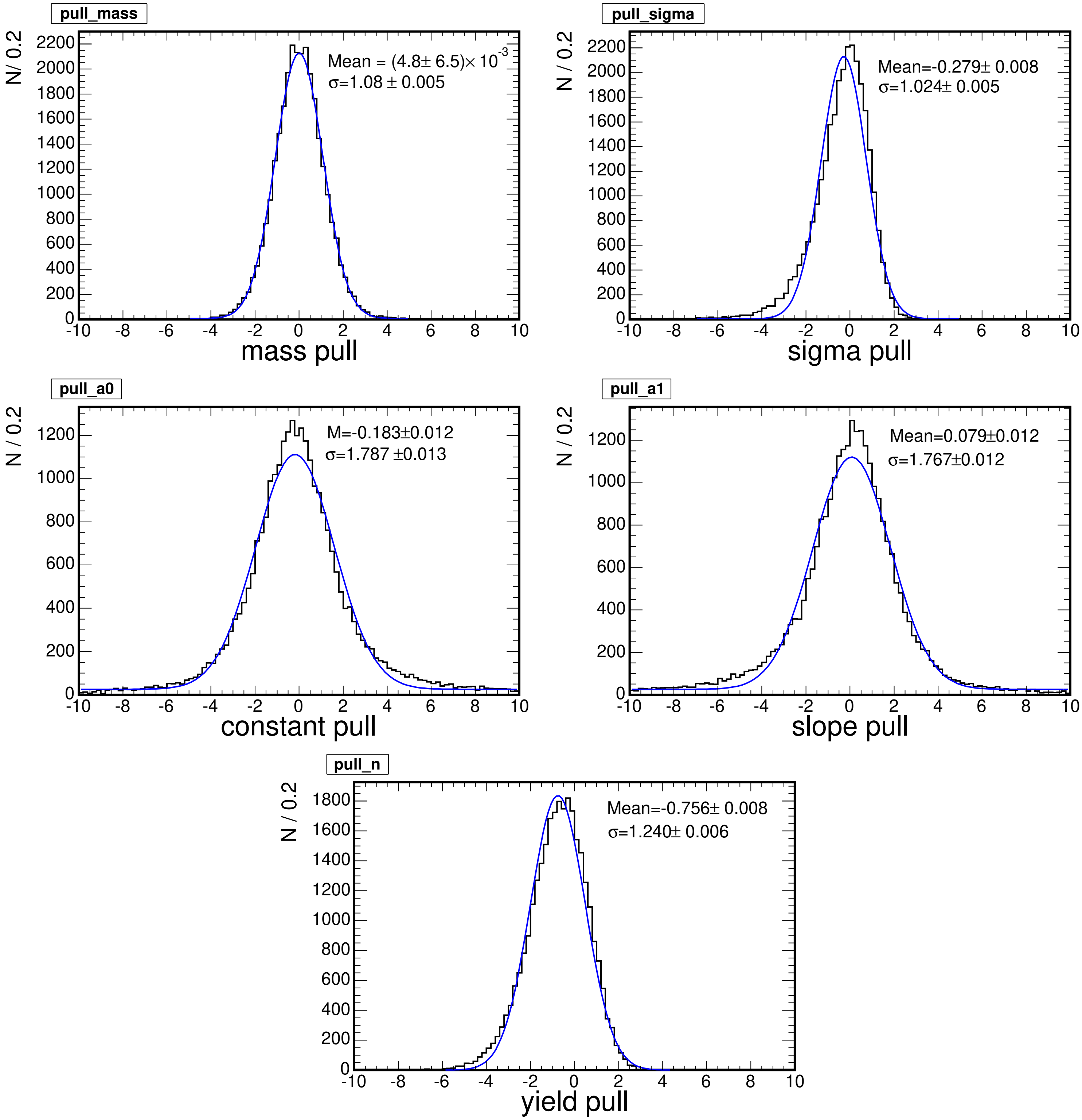


Figure 27: Fit Pulls

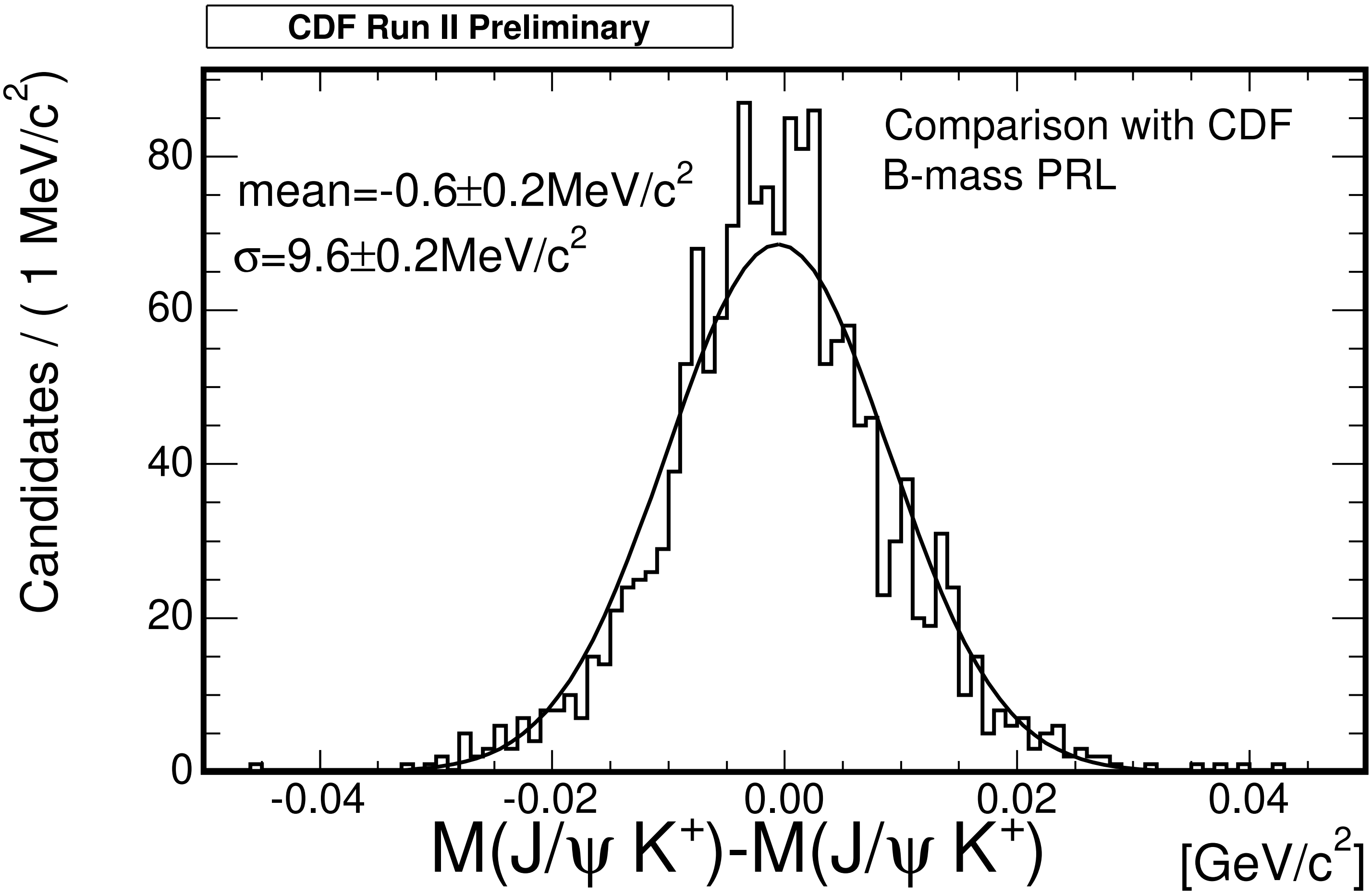


Figure 28: The event-by-eent mass difference of common events used in the CDF B Mass PRL for $B^+ \to J/\psi K^+$ and events found in this analysis.

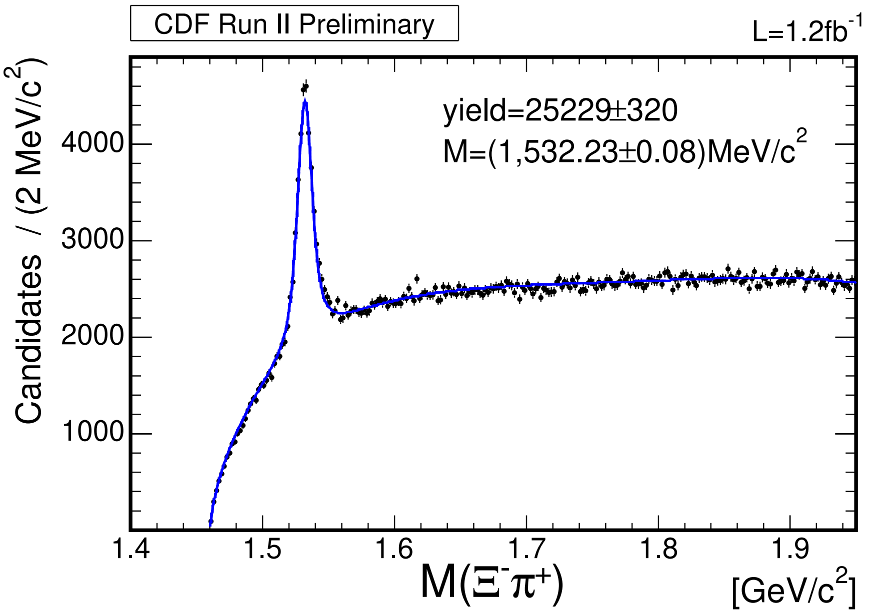


Figure 29: Invariant mass spectrum of $\Xi^-\pi^+$ combinations. Fit details are discussed in the text.

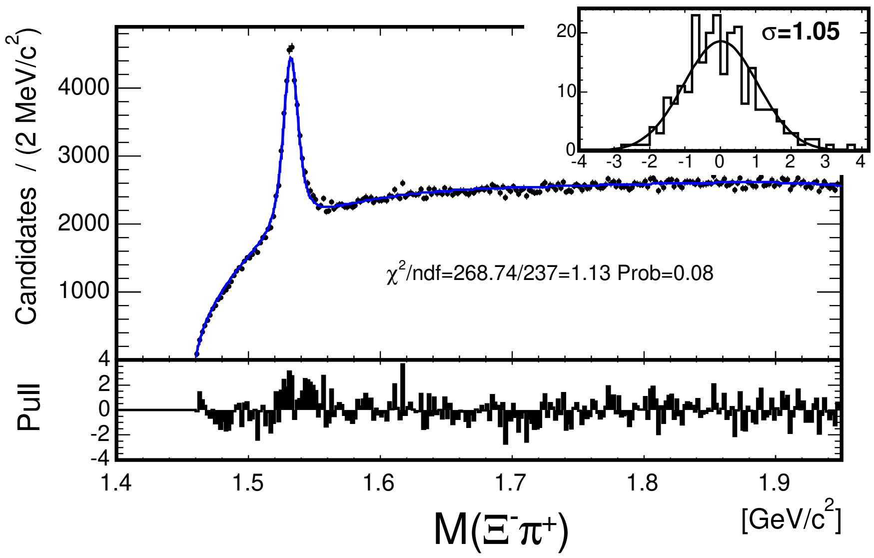


Figure 30: Invariant mass spectrum of $\Xi^-\pi^+$ combinations. Fit residuals.

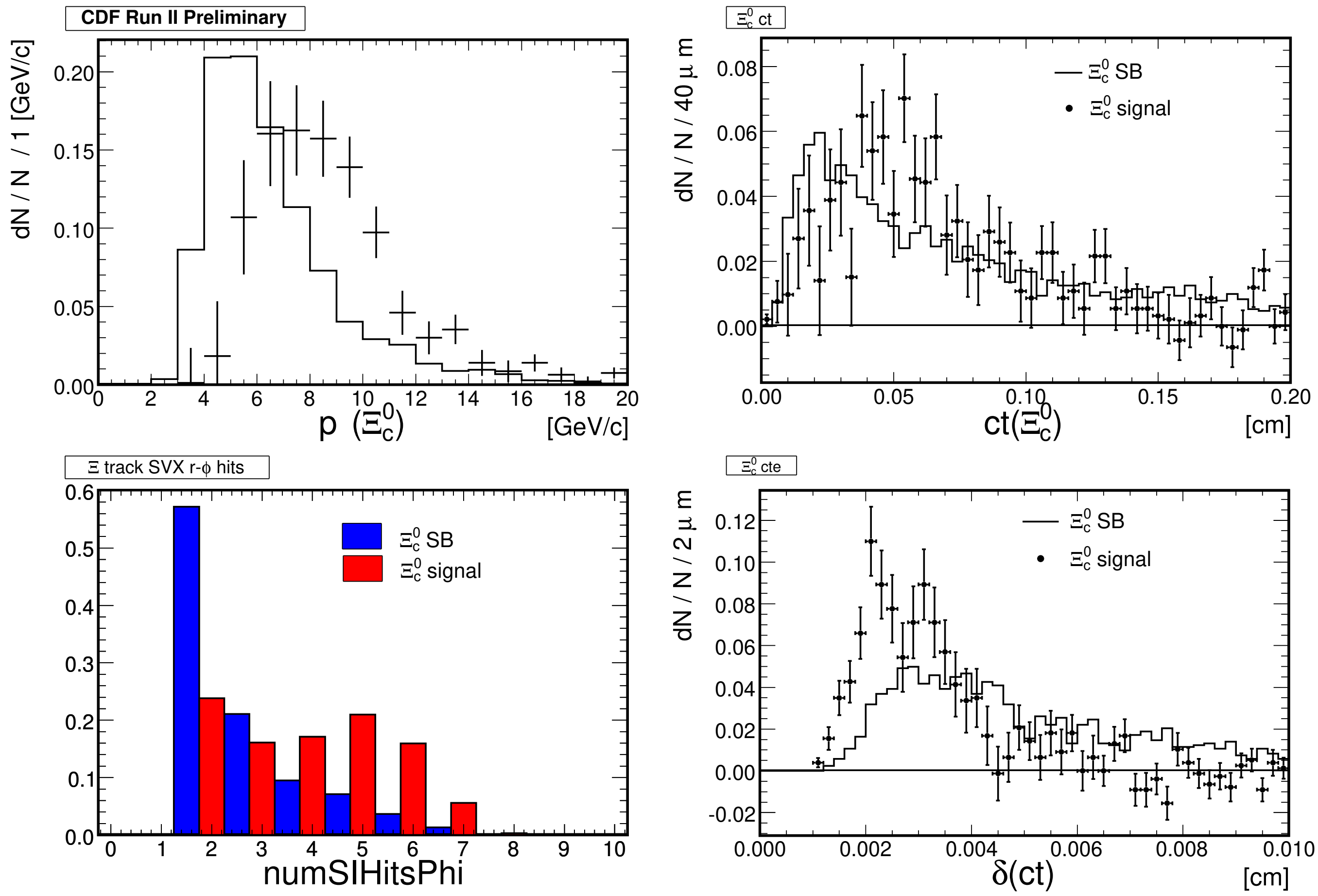


Figure 31: Variables used to select $\Xi_c^0$ candidates. Points with error bars signal region. Solid line histograms – sidebands.

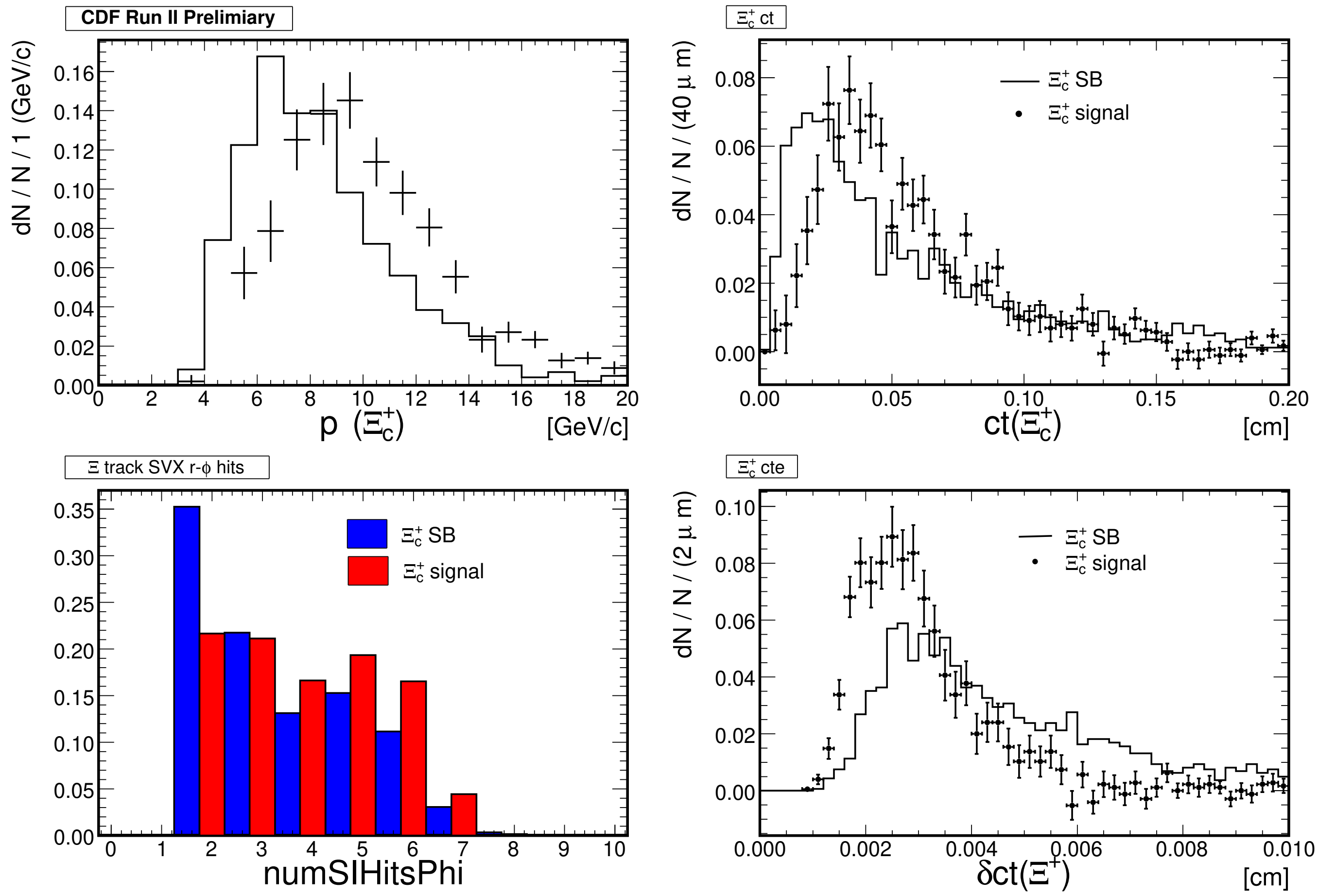


Figure 32: Variables used to select $\Xi_c^+$ candidates. Points with error bars signal region. Solid line histograms – sidebands.

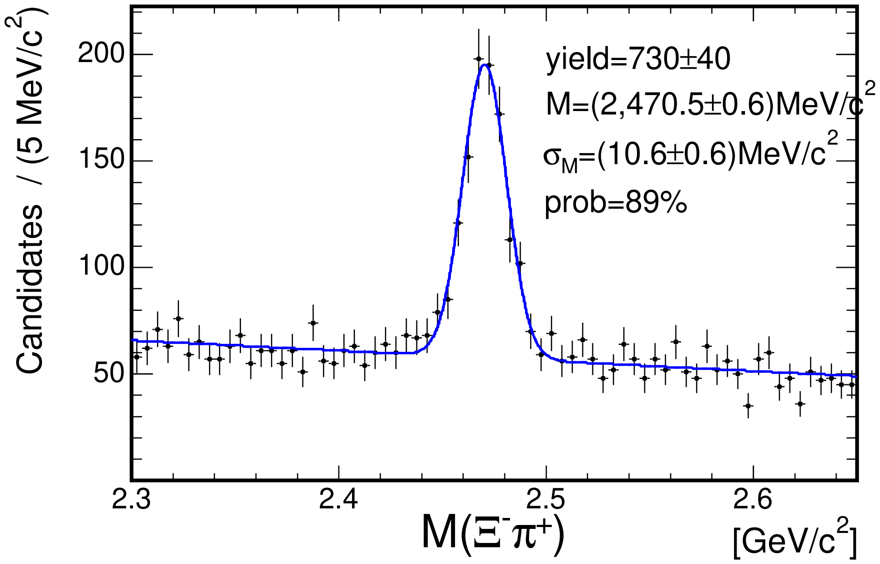


Figure 33: Invariant mass of $\Xi_c^0$ candidates.

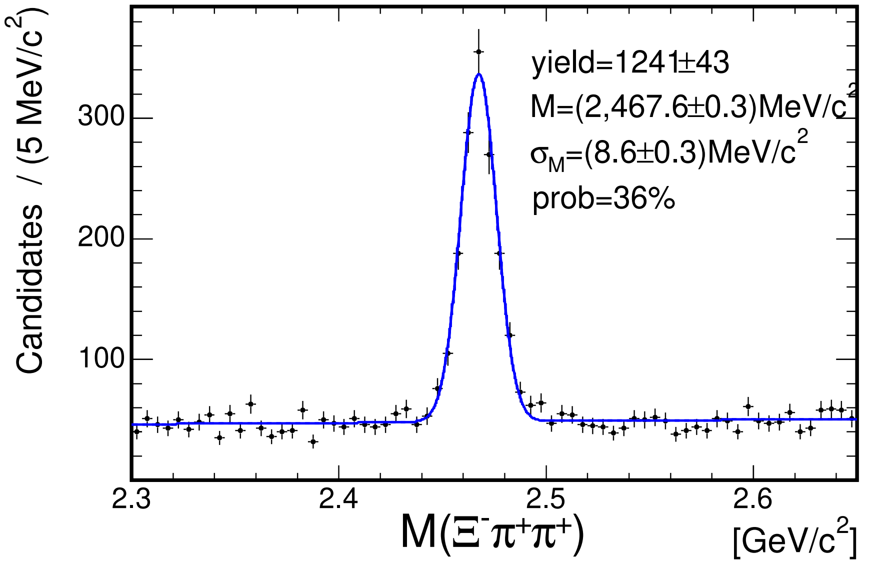


Figure 34: Invariant mass of $\Xi_c^+$ candidates.

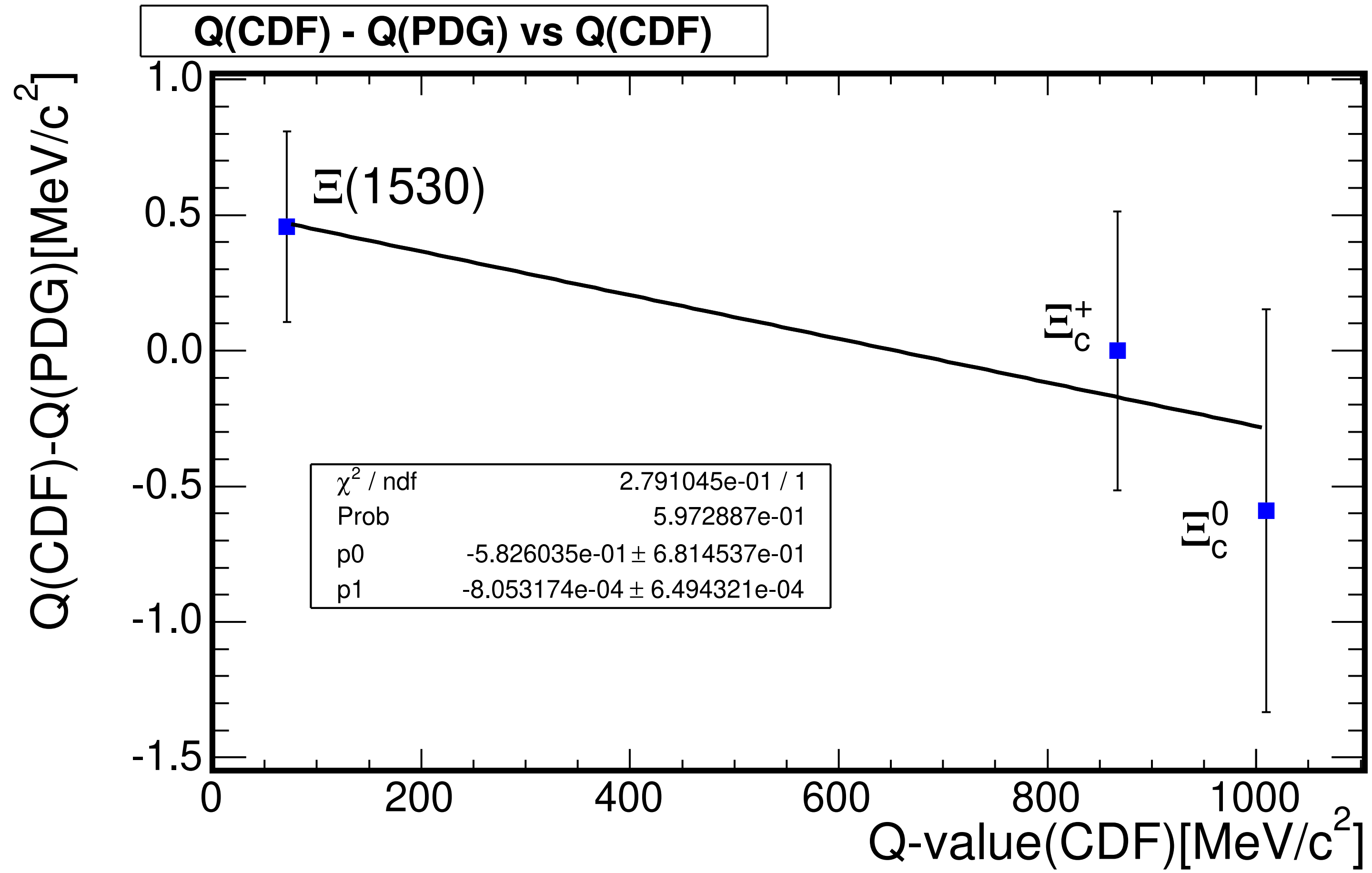


Figure 35: Summary of measured masses in TTT data